JOURNAL OF PETROLOGY | VOLUME 45 | NUMBER 4 | PAGES 759–792 | 2004 | DOI: 10.1093/petrology/egg109

Origin of Minette by Mixing of Lamproite and Dacite Magmas in Veliki Majdan, Serbia

D. PRELEVIĆ[1,2]*, S. F. FOLEY[1], V. CVETKOVIĆ[2] AND R. L. ROMER[3]

[1]INSTITUTE OF GEOLOGICAL SCIENCES, UNIVERSITY OF GREIFSWALD, JAHNSTRASSE 17A, D-17489 GREIFSWALD, GERMANY

[2]FACULTY OF MINING AND GEOLOGY, UNIVERSITY OF BELGRADE, ĐUŠINA 7, 11000 BELGRADE, YUGOSLAVIA

[3]GEOFORSCHUNGSZENTRUM POTSDAM, TELEGRAFENBERG, D-14473 POTSDAM, GERMANY

RECEIVED FEBRUARY 1, 2003; ACCEPTED SEPTEMBER 9, 2003

Composite dykes consisting of leucominette and dacite as well as discrete dykes and flows of minette and lamproite composition, occur in the Veliki Majdan area, western Serbia. This area is part of the Serbian Tertiary magmatic province, which consists of numerous small occurrences of ultrapotassic igneous rocks. The composite dykes have leucominette margins (up to 150 cm thick) enclosing a central part of dacite up to 100 m in width. Between these two lithologies, a decimetre-sized transition zone may occur. Petrography, mineral chemistry and bulk-rock geochemistry, including Sr, Nd and Pb isotopes, provide evidence that the minettes and leucominettes formed by hybridization between a felsic magma similar in composition to dacite and a mantle-derived lamproitic magma. The leucominettes and minettes contain all phenocryst types (biotite, plagioclase, quartz) present in the dacites, but in partly resorbed and reacted form. The mica displays a great diversity of resorption textures as a result of partial dissolution, incipient melting and phlogopitization, suggesting superheating of the felsic melt during hybridization; the mineral modes and mineral compositions of the leucominettes and minettes resemble those in the lamproites. A model for the modification of lamproite melt towards minette is presented in which minette is formed by mixing of lamproite and <30% felsic magma. The lack of any significant correlation between Pb isotopic ratios and some of the 'mixing-indices' (SiO_2, Zr, Zr/Nb, $^{143}Nd/^{144}Nd_i$) recognized in the hybridization model for the Veliki Majdan dykes may be a result of similarity of the Pb-isotopic signature in the two end-members. Highly phlogopitized biotite xenocrysts in the minettes are ascribed to the retention of volatile components after magma mixing and crystallization of a new generation of phlogopite from the hybridized magma. The magma-mixing model explains the reverse zoning and resorption features of phlogopite macrocrysts commonly recognized in calcalkaline lamprophyres elsewhere. Therefore, this mixing mechanism may be globally applicable for the origin of minettes associated with calcalkaline granitic plutonism in post-orogenic settings.

KEY WORDS: *Serbia; lamproites; micas; phlogopitization; calcalkaline lamprophyres; superheating; magma mixing*

INTRODUCTION

The idea that calcalkaline lamprophyres might originate by mixing of lamproites and crustally derived silicic melts was first proposed by Rock (1983, 1991), based on geochemical relationships. He suggested that within orogens, especially in areas of active granitoid plutonism, mantle-derived lamproite melts find passage through the continental crust very difficult and are usually thoroughly modified by the uptake of crustal components, resulting in the formation of minette melts. Although Rock suggested that this may be a common process, no comprehensive model of the modification process has been put forward, and very few natural examples in which this process can be observed are known.

Lamproites are rare, potassium-rich igneous rocks, strongly enriched in incompatible trace elements, but with high Mg number [100 × Mg/(Mg + Fe)] and high compatible trace element contents characteristic of mantle-derived melts (Jaques *et al.*, 1984, 1986; Foley *et al.*, 1987; Mitchell & Bergman, 1991). They are generally associated with intra-continental tectonic settings or post-orogenic collapse, post-dating convergent tectonics and active margin processes (Mitchell & Bergman, 1991).

*Corresponding author. Present address: Faculty of Mining and Geology, University of Belgrade, Đušina 7, 11000 Belgrade, Yugoslavia. Telephone and fax: +381-(0)11-630020.
E-mail: prelev@uni-greifswald.de

In the latter setting, lamproites may be associated with calcalkaline lamprophyres and calcalkaline silicic magmatism, so that the mixing of melts with contrasting composition might be expected in this environment.

Deciphering crustal assimilation and melt interaction involving lamproitic magmas is complicated by their high incompatible trace element concentrations relative to 'normal' basaltic melts. Furthermore, lamproites characteristically have Nd–Sr–Pb isotopes that may be further removed from those of the depleted upper mantle than are most continental crustal rocks (Vollmer *et al.*, 1984; Fraser *et al.*, 1985; Nelson *et al.*, 1986; Murphy *et al.*, 2002). The major effects of contamination of lamproitic magma by crustal components should be merely dilution of both compatible and incompatible elements with increasing degree of assimilation (Conticelli, 1998), because the concentrations of these elements are lower in the crustal rocks. In cases where no textural evidence for incomplete blending, resorption or the presence of xenolithic material is preserved, these chemical effects will, therefore, be difficult to recognize.

In this paper, we present the results of detailed geochemical, mineralogical and petrographic studies of four composite dykes comprising hybrid mafic and dacitic rocks from the Veliki Majdan area, western Serbia (Yugoslavia), as well as for nearby lamproites and a discrete minette dyke. These localities are part of a magmatic province of Tertiary age consisting of numerous small occurrences of ultrapotassic volcanic rocks, many of them lamprophyres and lamproites, as well as a whole spectrum of ultrapotassic rocks ranging from potassic trachybasalt to latite in composition (leucominettes) occurring in composite intrusions and as xenoliths in rhyodacite and quartz latite lavas (Prelević *et al.*, 2001*a*).

This study focuses on the genetic relationships between minette and lamproitic melts. We emphasize the significance of the high reactivity and potential for magma mixing of lamproitic melts. The hybrid rocks of Veliki Majdan show many types of reaction textures indicating incomplete equilibration, and provide evidence for an important role for magma mixing in the origin of calcalkaline lamprophyres. Finally, we present a comprehensive model by which lamproitic melts are involved in the origin of calcalkaline lamprophyres in general.

CALCALKALINE LAMPROPHYRES

Our understanding of the petrogenesis of lamprophyres is perhaps the poorest of any igneous rock group. The main reason for this is the confusion that reigns concerning their relationships with other rock and magma types. Systematic studies and groupings of lamprophyres were pioneered mostly by Rock (1977, 1983, 1986, 1991), who produced a series of publications aimed mostly at classifying the rocks and understanding their interrelationships. These works rationalized the previously existing confusing morass of local rock names, but have still left considerable ambiguities regarding their origins.

According to generally accepted earlier definitions (Wimmenauer, 1973; Rock, 1977, 1991; Streckeisen, 1978) lamprophyres are melanocratic hypabyssal igneous rocks with microporphyritic textures carrying hydrous mafic phenocrysts. Feldspars and other felsic minerals are restricted to the groundmass. The calcalkaline or shoshonitic lamprophyres received their group name from the common association with calcalkaline granitic rocks (Rock, 1977), and consist entirely of feldspar-bearing lamprophyres, excluding glassy, carbonate- and feldspathoid-dominated lamprophyres. Many are minettes, for which Mitchell (1994) proposed a redefinition to restrict its use to rocks associated with calcalkaline volcanism and plutonism. The term 'minette' thus survives the general terminological elimination of the lamprophyres by the IUGS subcommission on nomenclature (Woolley *et al.*, 1996; Le Maitre, 2002). The high modal phenocryst content, reverse zonation and resorption of macrocrysts in the most calcalkaline lamprophyres indicate a complex origin including crystal fractionation, hybridization and possibly accumulation of phenocrysts.

The lamproite connection

Although more than 160 examples of intimate associations between calcalkaline lamprophyres and granitoid rocks were reported by Rock (1991), only two have been thoroughly investigated: Caledonian appinites (Fowler & Henney, 1996) and Hercynian vaugnerites (Sabatier, 1991; Gerdes *et al.*, 2000; Ferré & Leake, 2001). The appinites are considered to represent plutonic spessartites and vogesites, whereas vaugnerites correspond to kersantites and minettes (Rock, 1991). Although the occurrence of lamproites in these associations has never been reported, the lamproitic affinity of these rocks is emphasized (Sabatier, 1991; Ferré & Leake, 2001), and is indicated by good correlations between MgO and K_2O, high K_2O/Na_2O ratio and low Al_2O_3 of the most primitive rocks. Nevertheless, even the most primitive representatives of the appinites and vaugnerites display many mineralogical, textural and geochemical features typical of hybridized rocks.

Rock's (1991) arguments for the modification of lamproite melts to minette in orogenic regions were based on geochemical similarities between crustally derived melts and the parental lamproitic melts, which he named M5. Contamination of Al-rich lamproite by peraluminous granite has been claimed for an unusual orthopyroxene-bearing minette suite from the eastern Andean Cordillera in Peru (Carlier *et al.*, 1997).

Mitchell & Bergman's (1991) attempts to define essential differences between lamproites and calcalkaline lamprophyres, especially minettes, are not entirely

convincing. Although they agreed that many minettes reported in the literature resemble high-silica lamproites in some aspects, they concluded that minettes and lamproites may be discriminated by the higher alumina contents in minettes, which lead to the diverging evolutionary trends of phlogopite compositions in minettes and lamproites. Also, lamproites are generally more enriched in incompatible trace elements. However, in our opinion, these differences are not substantial enough to claim that 'phlogopite phenocrysts are the only feature that these disparate rock types (lamproites and lamprophyres) have in common' (Mitchell & Bergman, 1991).

GEOLOGICAL SETTING OF THE VELIKI MAJDAN INTRUSIONS

Several composite dykes of Oligocene to early Miocene age (Delaloye *et al.*, 1989) occur in the Veliki Majdan area of western Serbia, and contain a large spectrum of ultrapotassic hybrid rock types. The Veliki Majdan locality is part of a Tertiary magmatic province comprising many small outcrops of ultrapotassic volcanic rocks related to the intracontinental post-collisional collapse and lithosphere delamination of the Dinaride orogen that followed the closure of Vardar Tethys at the end of the Mesozoic (Karamata & Krstić, 1996; Karamata *et al.*, 1997; Cvetković *et al.*, 2000*a*). The positions of the rocks of this magmatic province are shown superimposed on a map of the tectonic units of the Serbian part of the Balkan Peninsula in Fig. 1 together with the distribution of Tertiary plutonic and volcanic formations in Serbia, mostly of high-K–calcalkaline character.

Many of these ultrapotassic rocks are varieties of calcalkaline-lamprophyres and lamproites (Prelević & Milovanović, 1998; Cvetković *et al.*, 2000*b*; Prelević *et al.*, 2001*a*, 2001*b*, 2002), occurring as dykes, veins, small plugs, scarce lava flows, small volcanic cones and rarely as composite intrusions and xenoliths in acid volcanic rocks. Several lines of evidence demonstrate an essential role for magma mixing or mingling processes in the origin of the compositional variation in many of these ultrapotassic rocks: specifically composite intrusions in which gradations between mafic and felsic rock types are seen, lamprophyric xenoliths in dacites and rhyodacites, and reaction textures.

The samples considered here are parts of composite dykes and a discrete minette dyke from Veliki Majdan, as well as nearby silica-rich lamproite intrusions. The rationale for invoking a role for lamproitic melt in the origin of the Veliki Majdan composite intrusions and the minette dyke is that lamproites occur in close proximity to the composite intrusions and they are the most primitive ultrapotassic rocks of similar age. Also, the mineralogical and geochemical resemblance to minettes and leucominettes is exceptional.

The Veliki Majdan area is situated on the southeastern margin of the Oligocene granodiorite pluton of Boranja (Delaloye *et al.*, 1989), which belongs to the Dinaridic granitoid suite of Late Paleogene–Early Neogene age (Cvetković *et al.*, 2000*a*), and is situated on the border of three terranes—the Jadar block terrane, the Vardar zone composite terrane and the Drina–Ivanjica terrane (Karamata & Krstić, 1996; Karamata *et al.*, 1997). A swarm of dykes in the Veliki Majdan area penetrates basement mostly composed of Triassic limestones. Hydrothermal activity, which produced vein-type Pb–Zn deposits, is related to the Tertiary magmatism: all samples are taken from underground exposures in the Veliki Majdan Pb–Zn mine. No surface exposures of the composite dykes are known.

Composite dykes of dacite and leucominette composition range in width from a few metres up to 100 m. However, discrete dacite dykes of similar thickness are more common. We have identified more than 10 composite dykes and have investigated four in detail. They have marginal zones up to 1·5 m wide composed of leucominette, with dacitic rocks forming the much thicker central parts. A discrete subvertical minette dyke occurs in the Veliki Majdan area and cuts the same lithological units as the composite dykes and has a similar east–west orientation.

Lamproites form a distinct group amongst the ultrapotassic rocks of Serbia with petrological and geochemical features clearly resembling other Mediterranean-type lamproites (Prelević *et al.*, 2001*a*, 2002). Some lamproites occur in close proximity to composite bodies and minette dykes as very rare metre-sized dykes and remnants of lava flows. The nearest lamproite occurrence to Veliki Majdan is a relict of a small, silica-rich, lamproite lava flow situated about 50 km east at Zabrdica (Fig. 1). Another nearby occurrence with a lamproite dyke is at Rudnik. Dykes and lava flow relicts of similar composition are scattered in many small occurrences in central Serbia.

ANALYTICAL METHODS

Whole-rock major and trace (Cr, Ni, Co, V, Cu, Zn, Ba, Ga, Rb, Sr, Y, Zr and Nb) elements were determined by X-ray fluorescence (XRF) spectrometry on fused discs at the University of Greifswald. The sequential wavelength-dispersive Philips PW2404 X-ray spectrometer was equipped with a single goniometer-based measuring channel, covering the complete measuring range. Details of the accuracy and analyses of international standards using this method are given in the Appendix.

Whole-rock rare earth elements (REE), Li, Sc, Cs, Hf, Th and U were measured by inductively coupled plasma mass spectrometry (ICP-MS) at the University of Bristol under standard conditions using a VG PlasmaQuad PQ2 Turbo-plus ICP-MS system with a Meinhard Nebulizer.

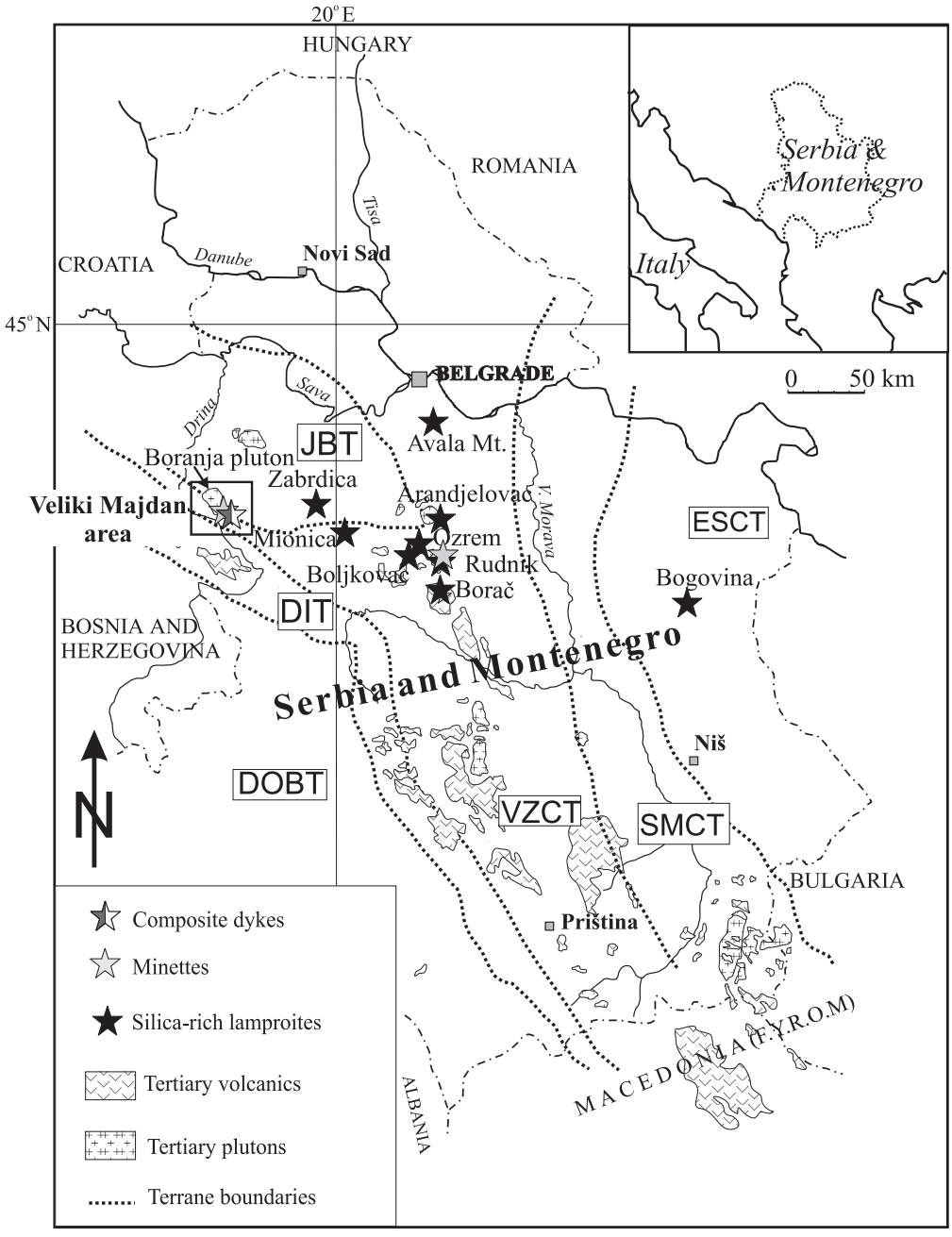

Fig. 1. Location of the study area together with occurrences of Serbian Tertiary lamproitic rocks. The locations of Tertiary plutonic and volcanic formations in Serbia (mostly of intermediate and acid calcalkaline composition) are also indicated. The terranes of the central part of the Balkan Peninsula are according to Karamata *et al.* (1999): ESCT, East Serbian composite terrane; SMCT, Serbo-Macedonian composite terrane; VZCT, Vardar zone composite terrane; JBT, Jadar Block terrane; DIT, Drina–Ivanjica terrane; DOBT, Dinaridic ophiolite belt terrane. F.Y.R.O.M., Former Yugoslav Republic of Macedonia.

Minerals were analysed using a JEOL 8900 RL wavelength-dispersive electron microprobe at the Geochemical Institute of the University of Göttingen and by a CAMECA SX 100 microprobe at the GeoForschungsZentrum Potsdam using PAP correction procedures. Counting times for all elements were 20 s for the peak position and 10 s for the background on each side of the peak. Operating conditions were 15 kV and 20 nA, and well-defined natural minerals were used as standards.

Whole-rock Sr and Nd isotopes were determined at the GeoForschungsZentrum Potsdam laboratories using procedures described by Romer *et al.* (2001). Samples were dissolved with 52% HF for 4 days at 160°C on a hotplate, and digested samples were dried and taken up in 6N HCl

overnight. Sr and Nd were separated and purified using cation-exchange chromatography. $^{87}Sr/^{86}Sr$ and $^{143}Nd/^{144}Nd$ were analysed on a VG 54-30 Sector and a Finnigan MAT262 multi-collector mass spectrometer, respectively, operated in dynamic mode. Ratios were normalized to $^{86}Sr/^{88}Sr = 0{\cdot}1194$ and $^{146}Nd/^{144}Nd = 0{\cdot}7219$, respectively. Multiple measurements of NBS 987 Sr reference material and La Jolla Nd reference material gave $0{\cdot}710277 \pm 0{\cdot}000009$ ($n = 4$) and $0{\cdot}511860 \pm 0{\cdot}000007$ ($n = 4$), respectively. Static $^{143}Nd/^{144}Nd$ values were adjusted to the value obtained for dynamic measurements ($0{\cdot}511850 \pm 0{\cdot}000004$, $n = 14$). Analytical uncertainties are reported as 2σ of the mean. $^{87}Sr/^{86}Sr_i$ and $^{143}Nd/^{144}Nd_i$ were calculated using known K–Ar ages, using $^{87}Rb = 1{\cdot}42E-11$ years^{-1} and $^{147}Sm = 6{\cdot}54E-12$ years^{-1}.

Pb from whole-rock samples was separated using anion exchange resin Bio Rad AG1-X8 (100–200 mesh) in 0·5 ml Teflon columns by HCl–HBr ion exchange chemistry using procedures described by Romer *et al.* (2001) and references therein. Pb was purified by a second pass over the column. Pb was loaded together with H_3PO_4 and silica gel, on single Re filaments. The isotopic composition of Pb was determined at 1200–1250°C on a Finnigan MAT262 multicollector mass spectrometer using static multicollection. Instrumental fractionation was corrected with 0·1% per a.m.u. as determined from repeated measurement of lead reference material NBS 981. Accuracy and precision of reported Pb ratios is better than 0·1% at the 2σ level.

PETROLOGY AND MINERAL CHEMISTRY

Composite dykes

The composite dykes are up to 10 m in width and comprise dacitic central parts with marginal parts of leucominette up to 1·5 m wide (see Fig. 7, below). There may be a decimetre-sized transitional zone between the felsic and mafic parts, indicating that they coexisted in partially molten form.

The leucominettes are dark grey microporphyritic rocks. They are composed of rare olivine phenocrysts (Fig. 2d), idiomorphic microphenocrysts and xenomorphic phlogopite, as well as variable amounts of biotite (Fig. 2a), quartz (Fig. 2c) and scarce plagioclase xenocrysts and resorbed amphibole. These are immersed in a microcrystalline phlogopite–quartz–alkali-feldspar groundmass. Numerous rounded vesicles containing epidote, phlogopite and chlorite also occur (Fig. 2b). We use the term leucominette (Wimmenauer, 1973) because of the clear compositional and modal resemblance of the samples to nearby minettes: these correspond to shoshonites and latites in terms of the total alkali–silica (TAS) diagram (Fig. 3; Le Maitre, 2002). Esperanca & Holloway (1987) used the term felsic minette for similar rocks.

In the leucominettes two generations of phlogopite can be distinguished: Type 1 are idiomorphic microphenocrysts of golden-yellow phlogopite (Fig. 2a), whereas Type 2 are pale yellow tabular to xenomorphic grains (Fig. 2a). The abundance of Type 1 phlogopite flakes correlates negatively with the modal abundance of biotite, quartz and plagioclase xenocrysts, and is least common in the most intensely hybridized rocks, where Type 2 clearly dominates. Type 2 phlogopite occurs as xenomorphic grains and sometimes as kinked microphenocrysts and groundmass plates but also as pseudomorphs after large biotite grains. They often exhibit dark skeletal outgrowths developing at the corners and rims (Fig. 2a and f).

Dacites have phenocryst contents of up to 60 vol. % quartz, biotite and plagioclase in an alkali feldspar and quartz matrix. The original igneous mineralogy is intensely altered and all samples contain calcite, sericite, chlorite and feldspar neoblasts. Tabular plagioclase phenocrysts are extensively pseudomorphed by alkali feldspar and sericite. The alteration is always polyphase: homogeneous pseudomorphs of alkali feldspar are superimposed by tiny flakes of sericite, calcite and rare quartz. Biotite comprises less than 10% of the original igneous mineralogy of the dacites, and is extensively pseudomorphed by chlorite, muscovite, calcite and leucoxene. This corresponds to the classical type of propylitic alteration (Jacobs & Parry, 1979). The alteration of the dacites in composite intrusions (but also in discrete dacitic dykes) is homogeneous in intensity and mineralogy.

In the leucominette, all phenocryst phases of the dacitic parts of the composite intrusions also occur. Here, they are fresh without signs of propylitic alteration and display reaction textures suggesting a xenocrystic origin (Fig. 2a and c). They exhibit a wide range of resorption textures: quartz has embayed rims and/or mantles of clinopyroxene sometimes with an intermediate zone of silica dendrites (Fig. 2c); feldspars are resorbed, and biotites show reverse zoning, incipient melting or other compositional heterogeneities (Fig. 2a) (see below). Leucominettes from different composite dykes have the same types of phenocrysts, but vary in modal xenocryst content and in the intensity of resorption textures, suggesting a similar origin but different extents of hybridization.

The decimetre-sized transitional zone that occurs at the contact between the felsic and mafic components in some intrusions is characterized by chemical gradations between the two lithologies. In other cases where the transition zone is absent, the composite intrusion has the appearance of a simple multiple intrusion. In both cases, mafic and felsic magmas coexisted, whereas commingling is apparent in the transition zones.

Representative microprobe analyses of minerals that occur in the leucominettes and the dacites from the

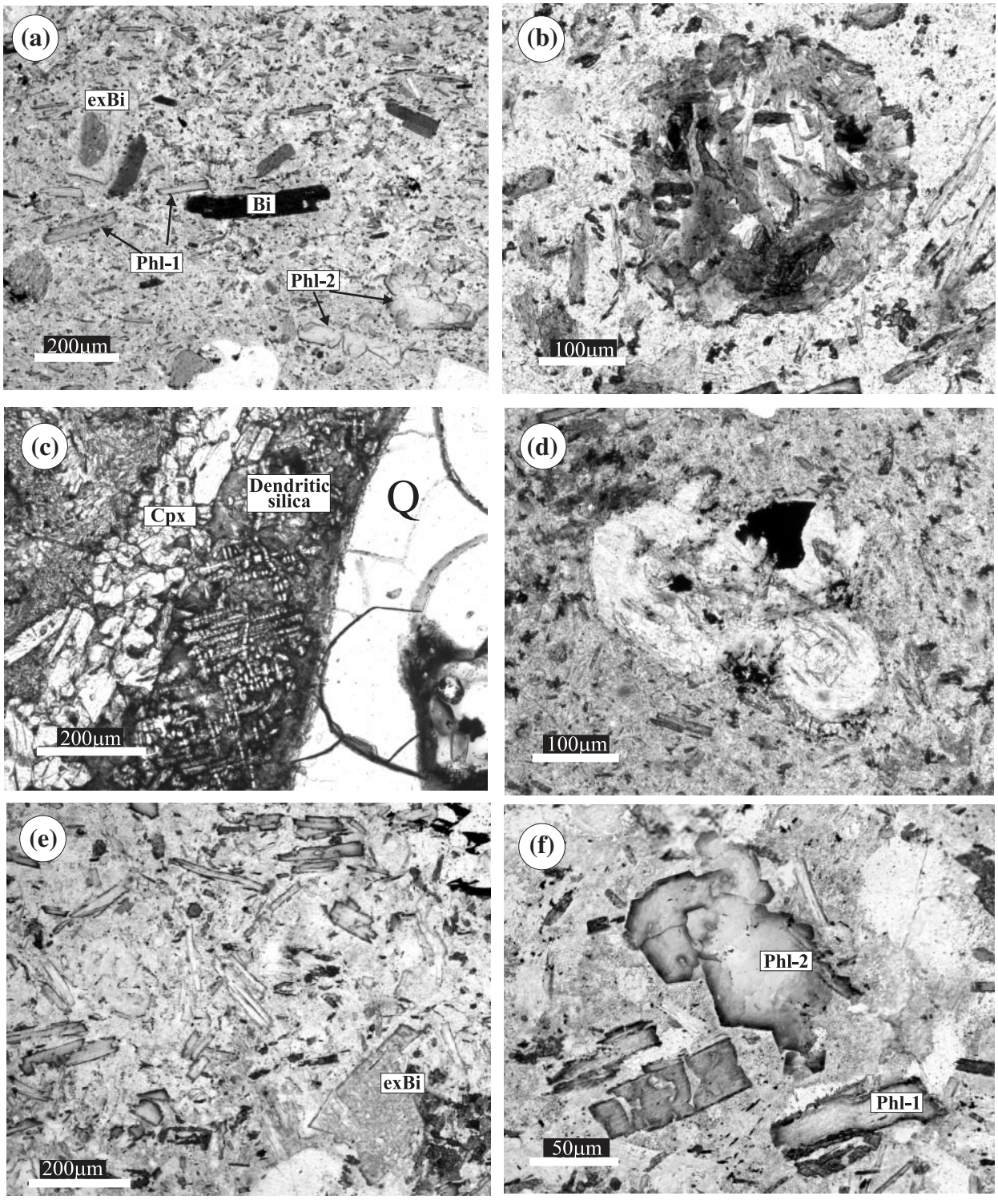

Fig. 2. Photomicrographs (plane-polarized light) of Veliki Majdan leucominettes (a–d) and minettes (e, f). (a) Typical appearance of leucominette with biotite plates (Bi), resorbed biotite (exBi) and Type 1 (Phl-1) and Type 2 (Phl-2) phlogopites; (b) vesicle filled with phlogopite + chlorite + Ti-magnetite; (c) quartz xenocryst mantled with clinopyroxene with an intermediate zone of dendritic silica crystals; (d) olivine phenocrysts in leucominette, completely pseudomorphed by iddingsite + chlorite + phlogopite + Ti-magnetite; (e, f) cumulophyric texture in minette. The Type 1 (Phl-1) and Type 2 (Phl-2) phlogopite and resorbed biotite xenocryst (exBi) should be noted.

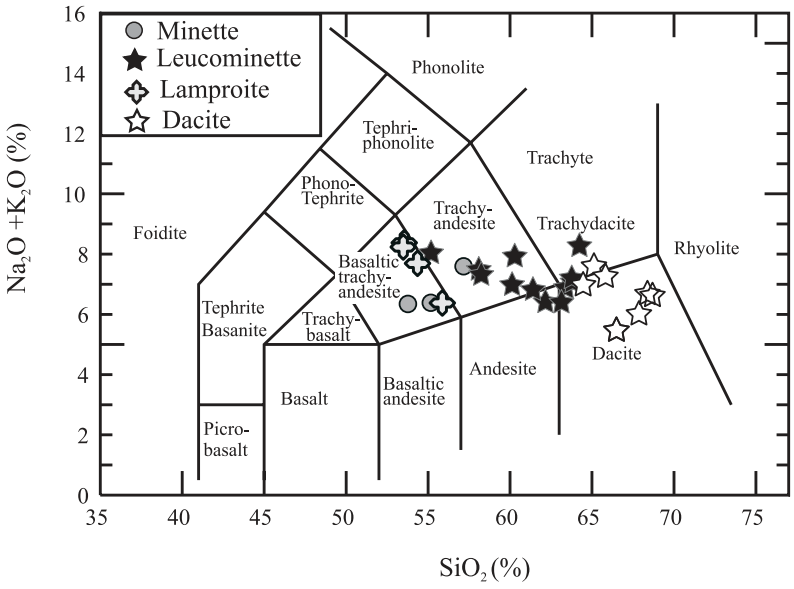

Fig. 3. Total alkali–silica classification diagram for investigated rocks (Le Bas *et al.*, 1986). Analyses are recalculated on a volatile-free basis.

composite intrusions are presented in Tables 1 and 2. We place emphasis on the micas because they are the key to understanding mixing relationships within the composite intrusions.

The composition of micas from the leucominettes varies widely, which is a characteristic for micas from calc-alkaline lamprophyres in general (Rock, 1991). The two phlogopite types recognized in the leucominettes display considerable compositional variations. Cores of phenocrysts (Type 1) have almost identical composition and compositional variation to Type 1 phlogopites from the minettes (see below), especially in terms of high Mg number, low Al and high Cr (Table 1). Type 2 phlogopites show a wide range of composition (Mg number 61–91), low Cr_2O_3 (<0·5%) and higher Al_2O_3 (up to 13·5%). Leucominette biotites have high Al_2O_3 contents (up to 15 wt %) and slightly lower Mg number (46) in comparison with biotite in minettes.

Rather small relicts of amphibole crystals occur rarely in the leucominettes; these are pargasitic amphibole with Mg number of 73 and relatively high K_2O/Na_2O ratios (Table 2).

Because of the intense propylitic alteration of the dacites, we have not been able to measure the unaltered composition of phenocrysts of plagioclase and biotite. Plagioclase is completely pseudomorphed by alkali feldspar and calcite, and biotite is chloritized. The secondary chlorite (Table 2) is devoid of systematic changes in tetrahedral Al occupancy within dacitic dykes, which is sensitive to temperature (Braxton & Petersen, 1999). This is in accordance with the homogeneity of the hydrothermal alteration of dacites.

Minettes

Minette is more melanocratic than leucominette (Fig. 2e), but has almost identical phenocryst and macrocryst types. Minette is composed of >40 vol. % phlogopite, biotite and olivine (which is replaced by iddingsite + chlorite + phlogopite + Ti-magnetite), and rare rounded and embayed quartz xenocrysts set in a groundmass of quartz and alkali feldspar. As in leucominettes, two morphological types of phlogopites are recognized (Fig. 2e). The xenomorphic Type 2 phlogopite clearly crystallized at a later stage and tends to form tabular crystals (Fig. 2f). Minette differs from leucominette in its higher abundance of Type 1 phlogopite phenocrysts. Hydrothermal alteration of primary minerals to chlorite, magnetite and alkali feldspar occurs irregularly. It is most probably related to the hydrothermal front from which a decimetre-sized vein of Pb–Zn ore at the contact of the minette dyke and Triassic limestone has been deposited.

The more melanocratic character of the minette gives the impression that it is more primitive than leucominette. However, the minette shows signs of evolved character and hybridization through the presence of rare resorbed quartz xenocrysts and biotite, revealing reaction textures similar to those in leucominette parts of the composite intrusions (Fig. 2e and f).

Representative analyses of minerals from the discrete minette dyke are presented in Tables 1 and 2. Here, cores of Type 1 phlogopite microphenocrysts and phenocrysts rimmed by magnetite aggregates have high Mg number (up to 92), high Cr_2O_3 contents (up to 2·0%) and low Al_2O_3 contents (around 12·0%). They display moderate zoning from core to rim, becoming richer in Al, Fe and

Table 1: Selected electron microprobe analyses of micas from composite dykes and minette dyke

Sample:	VM V/1-leucominette	VM VI/1-leucominette		VM V/1-leucominette	VM VI/1-leucominette	VM01/3-minette			VM01/3-minette		
	Phl-Type 1	Phl-Type 1	Phl-Type 2	Bi	Phlogopitized Bi	Phl-Type 1	Phl-Type 2	Phl-Type 2	Bi	Phlogopitized Bi	Phlogopitic rim Bi
SiO_2 (wt %)	41·32	41·20	38·79	37·02	38·15	40·43	40·38	39·98	37·07	37·48	40·55
TiO_2	2·12	2·03	4·01	3·65	3·36	2·01	2·17	2·82	3·49	3·46	2·71
Al_2O_3	12·47	12·86	13·40	14·32	14·83	12·58	13·55	13·50	14·57	14·64	13·05
FeO_t	3·27	3·38	13·25	19·46	10·90	3·38	3·58	9·92	17·40	8·99	8·88
MgO	24·87	24·78	17·03	12·38	18·38	24·40	23·60	20·99	13·75	19·70	21·52
MnO	0·03	0·02	0·17	0·37	0·14	0·01	0·07	0·07	0·33	0·06	0·07
Cr_2O_3	0·55	1·23	0·13	b.d.l.	0·01	1·33	1·70	0·05	0·02	0·05	0·08
CaO	0·55	1·23	0·02	b.d.l.	0·03	b.d.l.	0·06	0·05	0·01	0·03	0·03
K_2O	10·22	10·26	9·15	8·93	9·62	10·22	9·61	8·33	9·22	9·84	9·67
Na_2O	0·06	0·05	0·12	0·21	0·16	0·13	0·13	0·13	0·21	0·15	0·18
BaO	0·16	0·12	0·32	0·51	0·31	0·05	0·15	0·39	0·35	0·46	0·14
F	0·87	0·90	0·62	0·06	0·22	0·85	0·74	0·42	0·35	0·22	0·91
Total	96·48	98·04	97·00	96·91	96·11	95·39	95·74	96·65	96·77	95·07	97·79
Si	5·843	5·760	5·683	5·579	5·571	5·792	5·746	5·733	5·558	5·509	5·780
Ti	0·225	0·213	0·442	0·413	0·369	0·217	0·232	0·304	0·393	0·382	0·290
Al	2·079	2·119	2·314	2·545	2·552	2·124	2·273	2·282	2·575	2·537	2·192
TFe	0·387	0·395	1·624	2·452	1·331	0·405	0·426	1·190	2·182	1·105	1·059
Mg	5·242	5·165	3·720	2·780	4·001	5·211	5·006	4·487	3·073	4·317	4·573
Mn	0·003	0·002	0·021	0·047	0·018	0·001	0·008	0·009	0·042	0·008	0·009
Cr	0·062	0·135	0·015	b.d.l.	0·002	0·150	0·191	0·006	0·002	0·005	0·009
Ca	0·084	0·183	0·004	b.d.l.	0·004	b.d.l.	0·009	0·008	0·002	0·005	0·005
K	1·843	1·829	1·710	1·716	1·792	1·868	1·744	1·524	1·763	1·845	1·759
Na	0·016	0·013	0·033	0·061	0·045	0·036	0·036	0·036	0·061	0·042	0·050
Ba	0·009	0·007	0·018	0·030	0·018	0·003	0·008	0·022	0·021	0·026	0·008
Mg no.	93·1	92·9	69·6	53·1	75·0	92·8	92·2	79·0	58·5	79·6	81·2

Phl, phlogopite; Bi, biotite; cation proportions calculated on the basis of 22 oxygens; Mg number = 100Mg/(Mg + Fe) (atomic); b.d.l., below detection limit.

Table 2: Selected electron microprobe analyses of plagioclase, alkali feldspar, amphibole and chlorite from composite dykes and minette dyke

Sample:	VM XII/3-leucominette				VM01/3-minette		VM V/1-leucominette		VM VI/3-dacite	VM VI/4-dacite	VM VI/6-dacite
	plg. xeno.	plg. xeno.	plg. xeno.rim	alk. feld.	alk. feld. gm.		Amph xeno.		Chl	Chl	Chl
SiO_2 (wt %)	60·39	57·48	64·75	64·48	65·00	SiO_2 (%)	42·37	SiO_2 (%)	25·82	27·90	27·23
Al_2O_3	25·46	27·12	18·31	18·83	18·27	TiO_2	1·94	TiO_2	0·20	0·38	0·08
CaO	7·27	9·42	b.d.l.	0·11	0·07	Al_2O_3	12·15	Al_2O_3	18·74	19·57	18·64
FeOt	0·18	0·16	0·08	0·47	0·37	FeOt	10·16	FeOt	18·74	19·57	18·64
BaO	0·01	0·03	0·19	0·37	0·18	MgO	15·43	MgO	15·70	15·85	20·95
Na_2O	7·06	6·03	0·28	0·90	0·82	MnO	0·15	MnO	0·33	0·26	0·28
K_2O	0·67	0·44	15·66	14·73	15·02	Cr_2O_3	0·09	Cr_2O_3	b.d.l.	0·04	b.d.l.
Total	100·18	100·05	98·71	99·89	99·73	CaO	11·36	CaO	b.d.l.	0·04	b.d.l.
						K_2O	1·28	K_2O	0·10	0·66	b.d.l.
Si	10·675	10·259	12·027	11·914	12·014	Na_2O	1·85	Na_2O	0·03	0·01	0·01
Al	5·306	5·707	4·009	4·101	3·981	BaO	0·08	BaO	0·09	0·02	0·04
Ca	1·376	1·802	b.d.l.	0·023	0·014	Cl	0·02	Total	79·00	82·89	85·45
TFe	0·027	0·024	0·012	0·072	0·057	Total	96·89				
Ba	0·001	0·002	0·014	0·027	0·013						
Na	2·421	2·086	0·101	0·324	0·293			Si	5·804	5·930	5·663
K	0·152	0·100	3·710	3·472	3·540	Si	6·261	Ti	0·034	0·061	0·013
						Al^{IV}	1·739	Al^{IV}	2·162	2·009	2·324
						Al^{VI}	0·376	Al^{VI}	2·808	2·895	2·245
Or	0·04	0·03	0·97	0·91	0·92	Ti	0·216	Fe	3·523	3·479	3·241
Ab	0·61	0·52	0·03	0·08	0·08	Cr	0·011	Mg	5·260	5·024	6·496
An	0·35	0·45	b.d.l.	0·01	b.d.l.	TFe	1·255	Mn	0·062	0·047	0·050
						Mn	0·019	Cr	b.d.l.	0·006	b.d.l.
						Mg	3·399	Ca	b.d.l.	0·008	b.d.l.
						Ca	1·798	K	0·029	0·180	0·001
						Na	0·605	Na	0·014	0·005	0·005
						K	0·241	Ba	0·008	0·001	0·003
						Mg no.	0·73	^{VI}occup.	11·705	11·646	12·042
						P^* (kbar)	6·72				

plg, plagioclase; alk. feld, alkali feldspar; Amph, amphibole; Chl, chlorite; xeno., xenocryst; gm, groundmass. Cation proportions calculated on the basis of 32 oxygens for feldspars, 23 for amphibole, 28 for chlorite. ^{VI}occup., octahedral site occupancy; b.d.l., below detection limit.
*Pressure estimation using amphibole barometer of Hammarstrom & Zen (1986).

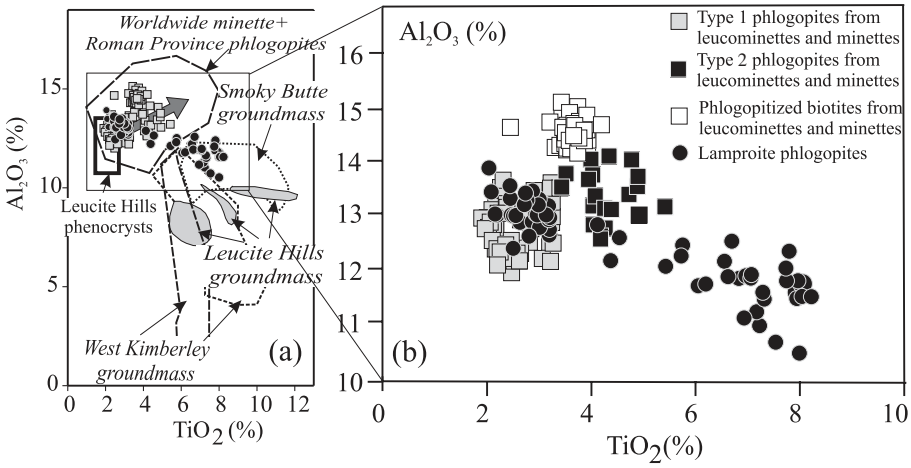

Fig. 4. (a) TiO_2 vs Al_2O_3 (wt %) diagram for phlogopites from leucominettes, minettes and lamproites. Data fields from Mitchell & Bergman (1991); wide grey arrow denotes typical evolutionary trend for phlogopites from calcalkaline lamprophyres and ultrapotassic rocks from the Roman Province (b). The inset shows that phlogopites from Veliki Majdan leucominettes and minettes exhibit a trend of increasing Al_2O_3 with increasing TiO_2 that is typical for calcalkaline lamprophyres and ultrapotassic rocks from the Roman Province. Phlogopites from Serbian lamproites evolve towards compositions with lower Al_2O_3 and higher TiO_2, following a typical lamproite trend as seen at Smoky Butte.

Ti, and poorer in Mg and Cr. The quench outgrowths at the corners and edges of the phlogopites have similar compositions to the Type 2 groundmass grains except for slightly higher Al_2O_3 (up to 13·6%) and lower Mg number (down to 79) and Cr_2O_3 contents. Coexisting biotite is mostly completely phlogopitized; rare exceptions have Mg number 57–78, no measurable Cr_2O_3 and high Al_2O_3 content (up to 15·0%). In leucominettes, biotite shows similar types of resorption to those in minette, but mostly with less intensity and with more abundant reverse zoning.

A summary of evolutionary trends and reaction textures in micas from leucominettes and minette

Phlogopites from Veliki Majdan leucominettes and minettes exhibit a core–rim trend of increasing Al_2O_3 content with increasing FeO_T and TiO_2 contents (Fig. 4). Similar trends are typical of calcalkaline lamprophyres and have been used to discriminate minette micas from those from lamproites and other ultrapotassic rocks (Mitchell & Bergman, 1991).

The reaction textures demonstrated by the investigated biotites from leucominettes and minette can be summarized as being of two types.

The first resulted from incipient melting of biotite and is characterized by a spongy texture, accompanied by varying degrees of pervasive replacement of biotite by phlogopite (Fig. 5e–g). This grades from grains with spongy cellular portions filled by glass similar to alkali-feldspar in composition and exsolution of tiny Ti-magnetites (Fig. 5e), through grains in which small islands of biotitic composition are preserved (Fig. 5f), to completely phlogopitized grains of high-alumina phlogopite composition (Fig. 5g). Similar features are seen in biotite xenocrysts from lamproites from southern Peru (Carlier *et al.*, 1994) and Spain (Toscani *et al.*, 1995). A similar example in pelitic gneiss enclaves entrained by doleritic magma was interpreted by Brearley (1987*a*, 1987*b*) to be caused by thermal breakdown and resorption of biotite. However, in this case, the magma was neither enriched in volatiles nor depleted in alumina, and therefore the decomposition products of biotite were magnetite, Al-spinel and melt. The chemical effects of this reaction are further illustrated by element-mapping of a sieve-textured biotite from a leucominette (Fig. 6). Element maps of Fe, Al, Ti, Cr and Si distribution show that the glassy patches and Ti-magnetite (red points on the Ti map) are distributed evenly throughout the grain. The area enclosing the melt pockets in the grain interior is now of phlogopitic composition (see Fe map), approaching the composition of high-Al Type 2 phlogopite. This phlogopitization process appears to be driven by the compositional contrast between biotite and the hybrid melt in which it is now enclosed.

The second type is indicated by strong and sudden reverse zonation of mica crystals from biotite cores to high-Al phlogopitic rims (Fig. 5e, c and a).

In Fig. 5, we arranged the back-scattered electron (BSE) images of resorbed biotites from leucominettes and minette according to the progression of intensity of reaction textures and degrees of hybridization indicated by their bulk whole-rock chemistry. The horizontal arrow denotes the degree of phlogopitization, which increases from left to right (the first type of the reaction textures). The phlogopitization is most intense in minette samples where already incipiently molten

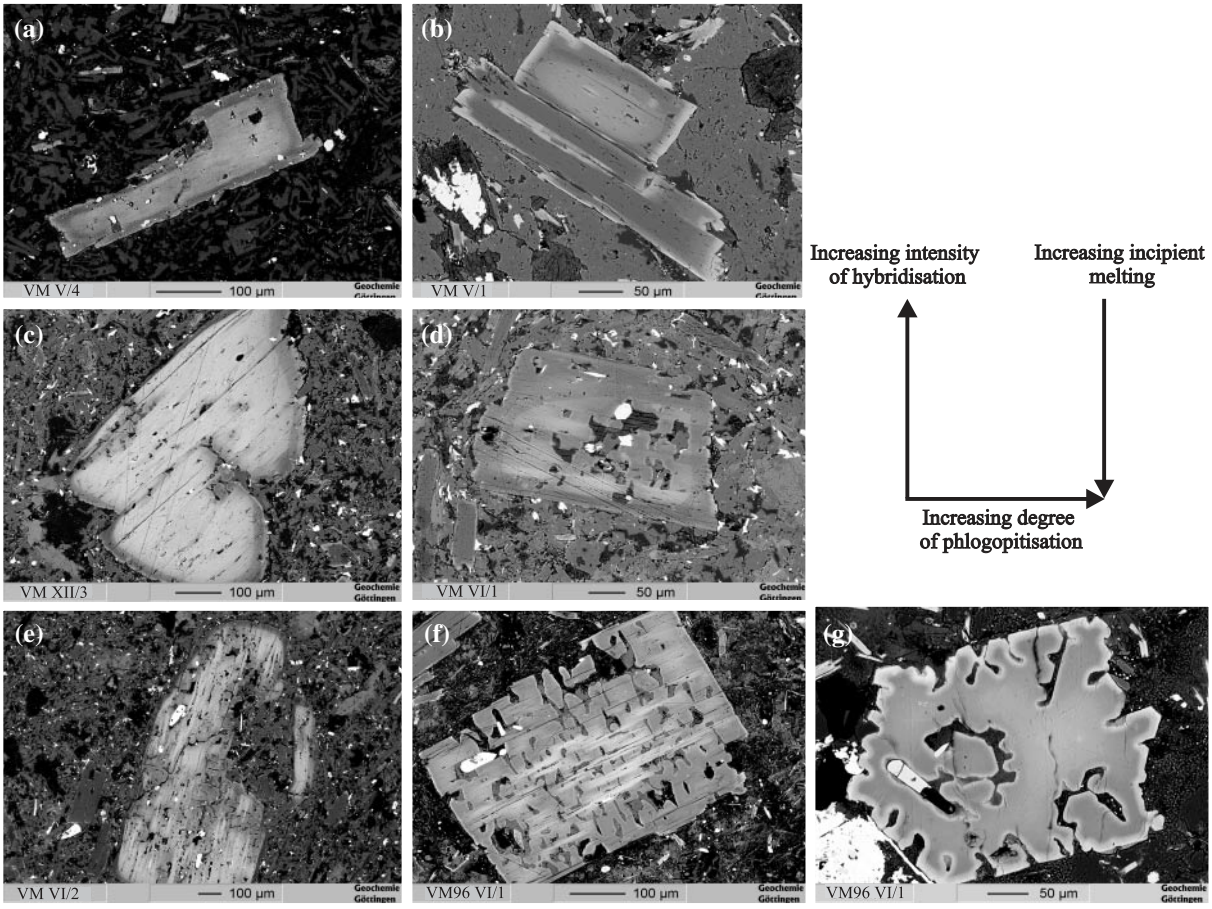

Fig. 5. BSE images of resorbed biotite xenocrysts from leucominettes and minette arranged according to the changing intensity of reaction textures. (a, b) Reverse zoning; (c, d) reverse zoning of biotite plates with different intensity of incipient melting; (e, f) more intense incipient melting superimposed on different levels of phlogopitization; (g) replacement of originally partially melted biotite by homogeneous high-Al phlogopite. The vertical arrow shows that the intensity of hybridization increases from the bottom towards the top. In the same direction, the intensity of incipient melting of biotite decreases. The horizontal arrow indicates the degree of phlogopitization, which increases from left to right. The phlogopitization is most intense in minette samples, with complete replacement of partially melted biotite by homogeneous high-Al phlogopite (f, g).

biotites are transformed to homogeneous high-Al phlogopites (Fig. 5f and g). The vertical arrow indicates increase of the intensity of hybridization from the bottom towards the top. In the same direction, the intensity of incipient melting of biotite decreases. In less mafic leucominettes, biotite xenocrysts exhibit sudden and reverse zonation resulting in rims of high-Al phlogopite (Fig. 5a). Phlogopitization and incipient melting of the biotite cores does not occur in these cases. The reverse zonation may mantle biotites that had already experienced various degrees of incipient melting and pervasive phlogopitization (Fig. 5f, d and b).

Lamproites

The lamproites studied here from Zabrdica and Rudnik are olivine–leucite and phlogopite–sanidine lamproites. They have phenocrysts of olivine and phlogopite set in a groundmass of sanidine, leucite, apatite, ilmenite, Cr-spinel, Ti-magnetite and rare rutile. They are devoid of felsic xenocrysts.

Idiomorphic, tabular olivine phenocrysts are strongly altered to iddingsite. When fresh, olivine displays very primitive composition (Mg number up to 93; Table 3). Phlogopite phenocrysts are characterized by core compositions with Mg number up to 92, Al_2O_3 11·7–14·0 wt %, and Cr_2O_3 up to 2·0 wt %, very similar to the phlogopites in the minette (Table 4). However, their core–rim compositional trend is opposite to the trend observed in the micas from the leucominettes and minettes (Fig. 4). The lamproite phlogopites evolve towards lower Al, higher Fe and higher Ti contents, following a typical lamproite trend (Mitchell & Bergman, 1991).

Cr-spinels often occur as inclusions in olivine phenocrysts, typically comprising idiomorphic crystals up to 5 µm in size that mostly resisted the alteration that

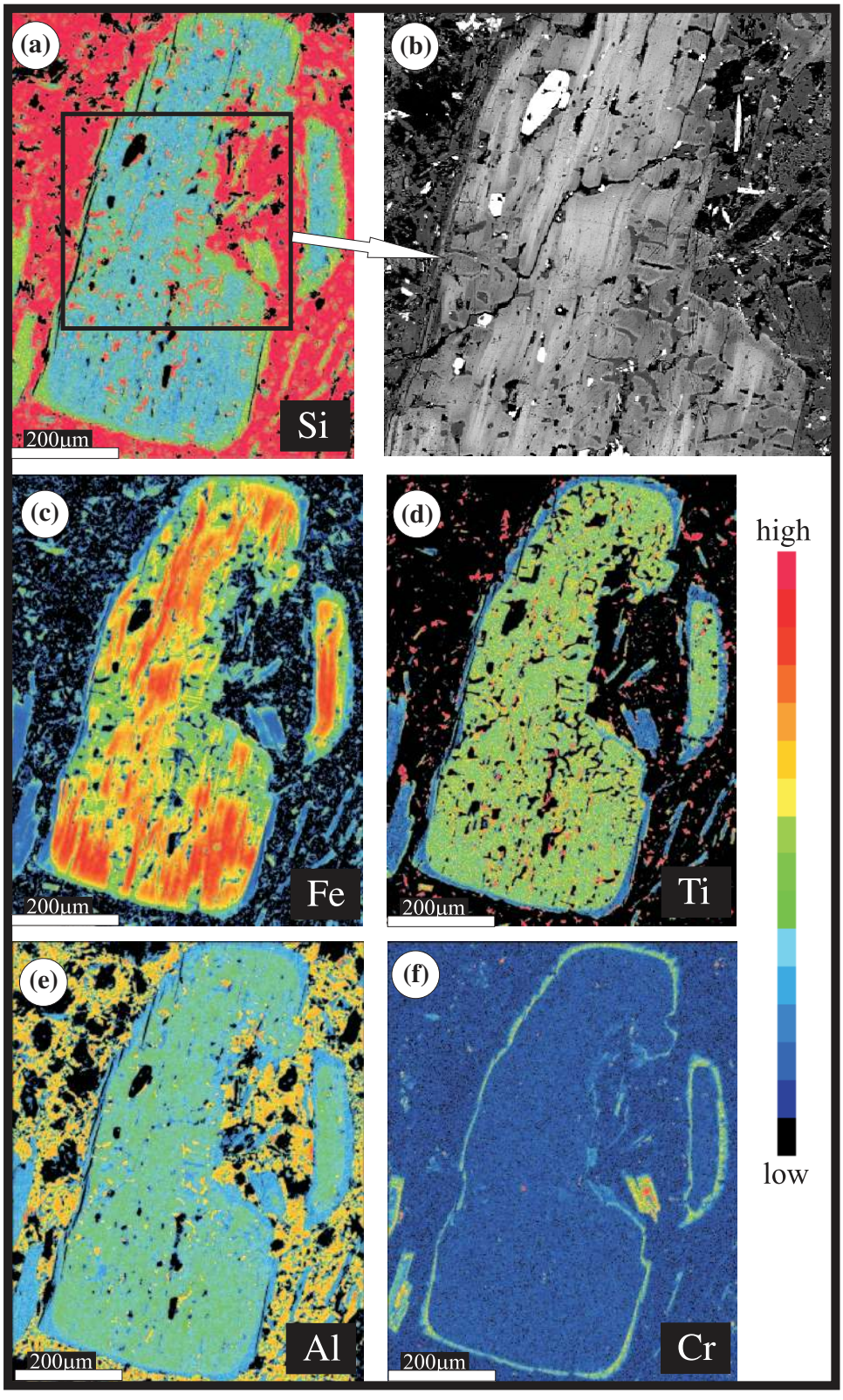

Fig. 6. Element-distribution maps (a, c, d, e and f) of a resorbed biotite xenocryst from leucominette sample VMVI/2. The same grain is enlarged in BSE image (b). Glassy patches (melt inclusions similar to alkali feldspar in composition) and Ti-magnetite grains (red points on the Ti distribution map) are distributed evenly throughout the grain and enclosed by high-Al phlogopite.

Table 3: Selected electron microprobe analyses of olivine, Mg-chromite, ilmenite, Ti-magnetite and alkali feldspar from lamproites

Sample:	Zb01/2					Ro01/1					Ro01/1		Zb01/2			Ro01/1		
	Ol-c	Ol-r	Ol-c	Ol-r		Mg-chromite					Ilmenite		Ti-magnetite			Alkali feldspar		
SiO_2 (wt %)	41·64	41·20	41·73	40·41	SiO_2	0·15	0·24	1·02	0·07	SiO_2	2·88	1·28	0·94	1·42	SiO_2	63·34	63·95	62·59
TFeO	7·74	10·62	8·40	14·67	TiO_2	1·24	1·09	1·37	1·06	TiO_2	47·57	47·14	15·44	15·51	Al_2O_3	16·10	17·23	17·11
MgO	50·54	48·65	50·36	45·13	Al_2O_3	7·62	6·47	5·60	2·92	Al_2O_3	1·06	3·23	0·60	0·66	MgO	1·96	0·05	3·70
MnO	0·10	0·17	0·12	0·27	TFeO	20·14	20·38	20·09	33·21	FeO	43·15	41·50	46·12	46·24	TFeO	2·91	1·77	1·48
CaO	0·13	0·21	0·15	0·19	MgO	9·95	10·18	11·27	5·53	Fe_2O_3	0·05	0·03	32·57	31·34	CaO	0·39	0·02	0·35
NiO	0·51	0·34	0·49	0·32	MnO	0·32	0·43	b.d.l.	0·62	MgO	0·69	0·22	2·38	2·41	K_2O	13·45	14·47	12·88
Total	100·15	100·84	100·76	100·67	Cr_2O_3	57·56	57·58	58·65	52·57	MnO	1·25	1·31	0·72	0·73	Na_2O	1·41	1·11	0·37
					CaO	0·01	0·02	b.d.l.	0·02	Cr_2O_3			0·03	0·06	BaO	0·13	0·24	0·04
Si	1·005	1·002	1·004	1·004	NiO	0·24	0·16	b.d.l.	0·02	CaO			0·42	0·49	Total	99·69	98·84	98·52
TFe	0·156	0·216	0·169	0·305	Total	97·22	96·55	98·00	96·01	NiO	0·64	0·76	0·06	0·05				
Mg	1·818	1·764	1·807	1·671						Total	97·23	95·45	99·27	98·91	Si	2·956	2·997	2·924
Mn	0·002	0·004	0·002	0·006	Si	0·041	0·065	0·275	0·019									
Ca	0·003	0·005	0·004	0·005	Ti	0·254	0·227	0·279	0·233						Al	0·886	0·952	0·942
Ni	0·010	0·007	0·009	0·006	Al	2·456	2·107	1·788	1·004	Si	0·141	0·066	0·282	0·429	Mg	0·136	0·004	0·257
					Fe	4·113	3·973	4·008	5·786	Ti	1·753	1·835	3·499	3·513	TFe	0·114	0·069	0·058
Fo	92·1	89·1	91·4	84·6	Fe^{3+}	0·497	0·733	0·542	2·309	Al	0·061	0·197	0·212	0·236	Mn			
					Mg	4·058	4·189	4·552	2·403	Fe	1·769	1·795	11·625	11·648	Ca	0·019	0·001	0·017
					Mn	0·075	0·100	b.d.l.	0·153	Fe^{3+}	0·149	0·001	7·386	7·105	K	0·801	0·865	0·768
					Cr	12·453	12·569	12·559	12·116	Mg	0·050	0·017	1·071	1·081	Na	0·127	0·101	0·033
					Ca	0·002	0·005	b.d.l.	0·006	Mn	0·052	0·057	0·184	0·186	Ba	0·002	0·004	0·001
					Ni	0·052	0·035	b.d.l.	0·005	Cr			0·007	0·015				
										Ca			0·135	0·157				
					Cr no.	0·835	0·856	0·875	0·923	Ni	0·025	0·032	0·014	0·013				

c, core; r, rim. Cation proportions calculated on the basis of four oxygens for olivine (Ol), 32 for spinel and Ti-magnetite, six for ilmenite, six for feldspar. Spinel Cr number = Cr/(Cr + Al). Fo = 100 × Mg/(Mg + Fe) (atomic). b.d.l., below detection limit; Fe_2O_3 recalculated according to stoichiometry.

Table 4: Selected electron microprobe analyses of phlogopite from lamproites

Sample:	Zb01/2						Ro01/-II									
	gm	1-core	1-rim	2-core	2-core	2-rim	core	gm	1-rim	1-rim	1-core	1-core	1-core	1-core	1-core	1-rim
SiO_2 (wt %)	39·74	40·12	40·07	40·32	40·11	41·16	40·06	40·16	38·39	39·25	40·22	40·42	40·81	41·24	40·51	37·73
TiO_2	6·64	5·63	6·15	6·18	5·89	6·16	4·48	7·51	7·04	6·66	2·85	2·92	2·68	2·63	2·65	8·20
Al_2O_3	11·84	11·46	11·12	11·55	11·50	10·80	12·63	10·71	11·95	12·56	13·07	13·33	13·32	13·24	13·45	11·54
TFeO	7·95	7·14	8·20	7·76	7·38	8·46	7·47	11·67	14·60	9·77	5·12	7·52	5·27	4·61	6·42	14·90
MgO	19·52	20·13	18·85	19·67	20·09	18·90	20·91	16·61	14·50	18·13	22·74	21·25	23·34	23·33	22·40	13·61
MnO	0·07	0·05	0·11	0·06	0·08	0·11	0·06	0·06	0·12	0·07	0·03	0·01	0·06	0·05	0·07	0·13
Cr_2O_3	0·09	0·11	0·03	0·01	0·02	0·01	0·57	0·15	0·02	0·05	1·65	1·66	0·62	1·07	0·84	0·01
CaO	0·13	0·78	1·54	0·20	0·21	1·14	0·01	b.d.l.	0·12	0·05	0·08	0·01	0·04	0·02	0·01	0·08
K_2O	9·26	9·16	9·02	9·36	9·48	8·58	9·73	9·15	8·99	9·30	9·55	8·75	8·87	8·61	8·23	8·80
Na_2O	0·63	0·60	0·62	0·62	0·68	0·56	0·25	0·45	0·42	0·30	0·24	0·22	0·17	0·16	0·21	0·46
BaO	0·25	0·13	0·20	0·17	0·15	0·14	0·26	0·45	0·65	0·46	0·12	0·16	0·16	0·05	0·13	0·96
F	2·69	2·87	2·63	2·74	2·82	2·37	3·12	2·02	2·47	2·35	3·29	3·14	1·84	2·08	3·00	2·26
Total	98·84	98·20	98·58	98·66	98·43	98·42	99·57	98·95	99·27	98·97	98·96	99·41	97·18	97·09	97·92	98·69
Si	5·712	5·790	5·792	5·794	5·781	5·906	5·727	5·823	5·670	5·663	5·729	5·752	5·788	5·836	5·783	5·624
Ti	0·718	0·611	0·668	0·667	0·638	0·665	0·481	0·819	0·782	0·722	0·305	0·312	0·286	0·280	0·284	0·919
Al	2·006	1·949	1·894	1·957	1·954	1·826	2·128	1·830	2·081	2·136	2·194	2·236	2·226	2·208	2·262	2·028
TFe	0·955	0·862	0·991	0·933	0·890	1·015	0·893	1·415	1·803	1·178	0·610	0·895	0·626	0·546	0·766	1·857
Mg	4·183	4·332	4·062	4·215	4·318	4·043	4·456	3·590	3·192	3·900	4·829	4·508	4·935	4·922	4·768	3·024
Mn	0·009	0·006	0·013	0·007	0·010	0·014	0·007	0·007	0·015	0·008	0·004	0·001	0·008	0·006	0·009	0·017
Cr	0·010	0·013	0·003	0·001	0·002	0·002	0·065	0·017	0·002	0·005	0·186	0·186	0·070	0·120	0·095	0·001
Ca	0·020	0·120	0·239	0·031	0·033	0·175	0·001	b.d.l.	0·018	0·008	0·012	0·002	0·006	0·002	0·002	0·012
K	1·698	1·687	1·663	1·717	1·744	1·570	1·775	1·692	1·695	1·712	1·736	1·588	1·605	1·555	1·498	1·673
Na	0·176	0·168	0·173	0·173	0·190	0·156	0·070	0·126	0·120	0·084	0·066	0·061	0·045	0·043	0·058	0·133
Ba	0·014	0·007	0·012	0·009	0·009	0·008	0·015	0·025	0·037	0·026	0·007	0·009	0·009	0·003	0·007	0·056
Mg no.	81·4	83·4	80·4	81·9	82·9	79·9	83·3	71·7	63·9	76·8	88·8	83·4	88·7	90·0	86·2	62·0

Cation proportions calculated on the basis of 22 oxygens. gm, groundmass; Mg number = 100 × Mg/(Mg + Fe) (atomic). b.d.l., below detection limit.

affected most of their host olivines. They are dominated by magnesiochromites (Table 3) with Cr number [Cr/(Cr + Al)] ranging up to 0·92 and $Fe^{3+}/\Sigma Fe$ 0·10–0·30, compositions that approach those of diamond inclusions, chromites associated with diamondiferous kimberlites and lamproites (Barnes & Roeder, 2001). Based on the equilibrium composition of coexisting Ti–Fe oxides using QUILF software (Andersen *et al.*, 1993), $\log f_{O_2}$ is estimated to be around FMQ − 2·1 (where FMQ is the fayalite–magnetite–quartz buffer).

Feldspar in the groundmass is mostly sanidine with up to 3% FeO_t (Table 3), a common feature of lamproites (Mitchell & Bergman, 1991). Leucite microphenocrysts are universally transformed to analcime, as is typical also for other Serbian ultrapotassic rocks (Prelević *et al.*, 2001*b*). Rutile, ilmenite and Ti-magnetite form tabular accessory grains not larger than 10 μm (Table 3). Further details about the mineralogy and geochemistry of lamproites from other Serbian localities have been given elsewhere (Prelević *et al.*, in preparation).

GEOCHEMISTRY

Analyses of whole-rock major (%) and trace elements (ppm) as well as Sr, Nd and Pb isotope compositions of samples from the Veliki Majdan composite dykes, minette dyke and nearby lamproites are presented in Tables 5 and 6. Lithological and chemical cross-sections through two composite dykes are presented in Fig. 7.

Major and trace elements

Leucominettes, minettes and lamproites are ultrapotassic rocks with K_2O >3%, MgO >3% and K_2O/Na_2O >2 (Foley *et al.*, 1987), whereas the dacites are high-K calcalkaline peraluminous silica-rich rocks. Major element oxide and trace element contents range widely from minettes and leucominettes to dacites: 50–65% SiO_2, 11–16% Al_2O_3, 8–2% MgO, 18–2% total Fe as Fe_2O_3, 8–3% K_2O, 1·2–0·5% TiO_2, 550–20 ppm Cr, 300–10 ppm Ni, 600–160 ppm Zr and 2200–800 ppm Ba. Leucominettes from different composite intrusions display a wide range of variation: almost every mafic member of composite dykes has a distinct composition.

The minette dyke possesses most of the characteristics ascribed to near-primitive mantle melts, with Mg number up to 69, and high Cr and Ni (up to 450 and 200 ppm, respectively). Normalized incompatible trace element patterns (Fig. 8) display generally similar patterns for leucominettes and minettes, with enrichment in Ba, Rb and Cs more than 1000 × primitive mantle, and high values of large ion lithophile element to high field strength element ratios (LILE/HFSE). Troughs are evident at Nb, Ti, Sr, Ba and P, whereas peaks of variable size are present at Pb. Leucominettes and minettes have very similar REE patterns with slight negative Eu anomalies. The level of enrichment of REE and the size of the Eu anomaly decrease from minette through leucominettes to dacites. Some of the dacite samples exhibit heavy REE (HREE) lower than 10 × chondrite.

Selected whole-rock analyses of lamproites are presented in Table 5. They have primitive characteristics with high Mg number (73–80) and high Cr and Ni, up to 850 and 530 ppm, respectively. They are mostly silica saturated without normative feldspathoids, but with a very small amount of normative quartz (<1%). Low Al_2O_3 content (mostly around 10 wt %) is a common feature of lamproites (Mitchell & Bergman, 1991). LILE/HFSE ratios are extremely high, with Ba, Rb and Cs more than 1000 × primitive mantle; other troughs and peaks are similar to those for minettes and leucominettes (Fig. 8a). The trace element patterns shown by lamproites, minettes and leucominettes resemble those of silica-rich lamproites of the Mediterranean region (Spain and Italy, Fig. 8a) (Venturelli *et al.*, 1984*b*; Conticelli & Peccerillo, 1992).

Sr, Nd and Pb isotopic composition

Minettes, leucominettes and dacites from Veliki Majdan vary significantly with respect to $^{87}Sr/^{86}Sr_i$ vs $^{143}Nd/^{144}Nd_i$ values (Table 6), covering the full range between Serbian granites and central Serbian silica-rich lamproites (Fig. 9).

The dacites fall within the range of Serbian granites. The minette and leucominettes display similar $^{143}Nd/^{144}Nd_i$ values falling in a narrow range of 0·512223–0·512162, but show significant differences in $^{87}Sr/^{86}Sr_i$ values: leucominettes are typically around 0·710, whereas the minette lies at 0·713, and is more radiogenic than the Serbian lamproites. As a Pb–Zn ore vein occurs at the contact of the minette dyke with Triassic limestone, the most reasonable explanation for the more radiogenic Sr isotope composition could be the alteration of the minette triggered by the fluids from the hydrothermal front. To test whether the alteration of minette is responsible for increasing its $^{87}Sr/^{86}Sr_i$, we leached sample VM01/3 with acetic acid and measured the Sr isotope composition of the leachate. This gave 0·717445 ± 16, which clearly confirms the interpretation that alteration has raised its Sr isotopic ratio. This alteration affected only Sr isotopes noticeably, because of the greater mobility of Sr relative to Nd in hydrothermal fluids.

Serbian lamproites display a marked consistency and homogeneity in their Sr and Nd isotope composition and are restricted in the plot of $^{87}Sr/^{86}Sr_i$ vs $^{143}Nd/^{144}Nd_i$ to the area around 0·71155 and 0·512190, respectively (Fig. 9, Table 6).

Table 5: Whole-rock major (%) and trace element (ppm) analyses of rocks from Veliki Majdan composite dykes and minette dyke, as well as nearby lamproites

	Discrete dyke			Composite dyke 1				Composite dyke 2						
	Minette dyke													
				LM	LM	D	LM	LM	LM	D	D	D	D	LM
Sample:	VM01/3	VM01/1	VM96VI/1	VM V/1	VM V/2	VM V/3	VM V/4	VM VI/1	VM VI/2	VM VI/3	VM VI/4	VM VI/5	VM VI/6	VM VI/7
SiO_2 (wt %)	52·87	47·98	50·25	56·81	58·86	64·66	59·10	54·73	50·61	60·97	59·39	61·58	60·72	53·36
TiO_2	1·08	1·07	1·08	0·93	0·86	0·45	0·85	0·99	1·15	0·59	0·58	0·51	0·50	1·04
Al_2O_3	11·60	10·82	11·00	14·05	13·72	14·74	13·61	12·12	10·99	14·57	13·97	15·04	15·86	12·11
TFe_2O_3	11·57	18·16	14·26	4·43	4·37	2·74	3·82	3·59	4·35	2·97	3·00	2·95	4·07	2·28
MnO	0·09	0·14	0·09	0·09	0·09	0·05	0·09	0·13	0·18	0·09	0·10	0·08	0·08	0·15
MgO	7·27	5·35	8·10	4·87	4·59	2·09	4·19	5·73	7·55	3·12	3·40	2·51	2·07	2·64
CaO	1·42	1·19	1·21	4·32	3·93	3·16	4·31	6·17	9·33	4·14	5·22	4·07	3·14	9·55
Na_2O	0·51	0·12	0·04	0·14	0·95	1·94	0·55	0·21	0·30	1·87	1·17	2·55	0·54	0·09
K_2O	6·51	5·54	5·77	5·74	5·46	4·31	6·02	7·81	7·10	5·27	5·28	4·26	4·47	6·95
P_2O_5	0·66	0·63	0·66	0·43	0·41	0·20	0·42	0·53	0·61	0·29	0·29	0·25	0·23	0·55
LOI	6·08	8·67	7·62	7·38	5·86	4·39	7·23	7·51	7·54	5·72	7·19	5·86	7·66	11·28
Total	99·64	99·66	99·05	97·23	97·77	98·14	98·63	99·20	99·10	99·16	98·96	99·24	98·07	99·84
Cr (ppm)	384	394	420	233	210	60	201	341	454	108	116	59	19	371
Ni	257	236	213	91	108	28	145	196	257	56	71	30	10	212
Co	18	6	25	22	20	5	24	27	21	8	9	6	8	17
V	86	80	104	83	77	47	76	83	94	69	74	68	77	87
Cu	11	31	11	9	19	15	14	17	12	6	6	13	11	13
Zn	102	302	91	851	116	25	421	201	98	43	45	38	34	45
Ba	1853	1272	2159	956	917	879	857	1257	1007	1051	1017	1050	1030	1914
Ga	15	15	16	21	19	20	19	23	24	19	19	18	19	18
Li	46	36	56	—	—	—	—	32	35	—	—	52	—	35
Sc	12	12	12	—	—	—	—	13	14	—	—	8	—	12
Rb	260	315	263	340	319	231	351	337	380	243	260	191	200	275
Sr	307	324	300	274	358	411	294	590	587	498	382	569	249	418
Y	21	21	21	—	—	—	—	20	21	—	—	16	—	19
Zr	539	518	501	451	407	179	418	510	568	226	241	182	161	515
Nb	32	27	36	32	28	21	30	34	36	22	23	19	21	36
Cs	15·4	26·9	14·5	—	—	—	—	14·4	17·0	—	—	14·2	—	19·8
Hf	6·1	13·5	13·6	—	—	—	—	15·0	16·2	—	—	2·6	—	12·8

	Discrete dyke			Composite dyke 1				Composite dyke 2						
	Minette dyke													
Sample:	VM01/3	VM01/1	VM96VI/1	LM VM V/1	LM VM V/2	D VM V/3	LM VM V/4	LM VM VI/1	LM VM VI/2	D VM VI/3	D VM VI/4	D VM VI/5	D VM VI/6	LM VM VI/7
Pb	56	1171	49	39	21	42	18	46	74	22	19	32	25	50
Th	18·5	52·2	50·7	37	35	20	30	44·7	43·7	27	24	19·6	17	37·8
U	6·2	16·6	16·5	4	4	3	3	14·5	13·7	3	4	7	2	13·3
La	62·76	70·23	70·86	45	56	31	30	59·05	56·4	39	53	42·43	41·22	54·38
Ce	154·04	168·63	175·07	117	131	55	93	149·41	141	93	94	83·32	83·66	136·46
Pr	19·58	21·25	22·33	—	—	—	—	19·78	20·40	—	—	9·11	9·05	17·65
Nd	84·32	90·6	96·4	59	64	29	61	88·37	85·8	40	44	36·45	35·54	77·1
Sm	14·61	15·73	16·81	—	—	—	—	15·75	15·20	—	—	6·61	6·29	13·91
Eu	2·68	3·02	3·33	—	—	—	—	2·96	2·69	—	—	1·77	1·58	2·79
Tb	1·18	1·21	1·30	—	—	—	—	1·19	1·01	—	—	0·70	0·68	1·08
Gd	9·33	9·49	10·32	—	—	—	—	9·72	9·54	—	—	4·98	4·88	8·90
Dy	4·40	4·47	4·68	—	—	—	—	4·31	4·29	—	—	2·92	3·00	4·05
Ho	0·72	0·70	0·76	—	—	—	—	0·71	0·68	—	—	0·51	0·55	0·66
Er	1·84	1·79	1·82	—	—	—	—	1·77	1·79	—	—	1·37	1·45	1·68
Tm	0·24	0·25	0·24	—	—	—	—	0·23	0·23	—	—	0·20	0·21	0·22
Yb	1·56	1·57	1·56	—	—	—	—	1·49	1·40	—	—	1·18	1·30	1·52
Lu	0·23	0·22	0·23	—	—	—	—	0·22	0·22	—	—	0·18	0·20	0·20

	Composite dyke 3					Composite dyke 4					Zabrdica		Rudnik	
Sample:	LM VM XII/1	LM VM XII/2	LM VM XII/3	LM VM XII/4	D VM XII/5	LM VM XIV/2	LM VM XIV/4	D VM XIV/1	D VM XI/2	LM VM XIV/6	L ZB01/1	L ZB01/2	L Ro0/1-II	L Ro0/1-A
SiO_2 (wt %)	52·49	53·13	55·61	58·26	63·54	57·02	59·98	62·92	60·72	61·12	50·42	51·50	46·68	47·27
TiO_2	1·00	0·98	0·88	0·72	0·43	0·78	0·75	0·45	0·50	0·98	1·41	1·45	1·63	1·64
Al_2O_3	11·69	11·45	12·47	13·64	14·49	12·91	13·87	14·33	15·86	12·58	10·57	10·73	10·80	10·94
TFe_2O_3	4·47	4·42	4·60	4·04	2·57	4·57	3·80	4·06	4·07	3·50	6·83	7·28	7·04	6·95
MnO	0·16	0·16	0·14	0·10	0·08	0·11	0·10	0·04	0·08	0·09	0·07	0·10	0·08	0·07
MgO	7·43	7·47	6·76	4·90	1·99	5·71	3·99	1·76	2·07	4·51	8·50	10·30	9·84	10·40
CaO	6·31	6·90	5·60	4·75	3·59	5·40	4·72	3·68	3·14	4·33	6·84	6·30	3·82	3·82

Table 5: continued

	Composite dyke 3					Composite dyke 4					Zabrdica		Rudnik	
	LM	LM	LM	LM	D	LM	LM	D	D	LM	L	L	L	L
Sample:	VM XII/1	VM XII/2	VM XII/3	VM XII/4	VM XII/5	VM XIV/2	VM XIV/4	VM XIV/1	VM XI/2	VM XIV/6	ZB01/1	ZB01/2	Ro0/1-II	Ro0/1-A
Na_2O	0·11	0·14	0·59	1·41	1·38	1·37	1·53	2·10	0·54	1·42	1·77	2·96	0·57	0·55
K_2O	6·68	6·56	5·89	4·51	4·85	4·98	5·27	3·49	4·47	6·48	4·01	4·36	6·77	6·77
P_2O_5	0·46	0·45	0·39	0·31	0·20	0·45	0·40	0·23	0·23	0·45	0·52	0·52	0·70	0·71
LOI	8·75	8·57	7·06	7·35	5·97	6·53	5·71	6·67	7·66	4·46	8·56	4·06	11·19	10·15
Total	99·36	100·02	99·64	99·41	98·73	99·37	99·71	98·72	98·07	99·27	100·04	100·06	99·66	99·83
Cr (ppm)	537	532	420	309	66	290	220	44	19	258	802	837	695	689
Ni	273	257	206	144	24	176	101	20	10	137	465	427	486	530
Co	28	31	24	13	4	22	14	11	8	16	36	33	33	40
V	98	88	93	75	60	86	78	78	77	66	137	131	137	145
Cu	23	12	13	11	15	76	10	49	11	4	10	17	25	42
Zn	62	52	62	72	36	61	191	31	34	79	79	79	75	78
Ba	1259	1217	1072	898	1582	1060	1155	834	1030	1034	1128	826	1153	1119
Ga	18	19	19	17	19	18	18	18	19	18	16	18	17	17
Li	—	—	57	—	—	41	30	23	26	33	194	87	107	102
Sc	—	—	12	—	—	12	10	8	8	9	22	22	26	26
Rb	322	339	283	218	227	226	251	122	100	359	191	194	221	218
Sr	408	400	399	513	379	450	490	346	325	417	608	586	598	599
Y	—	—	18	—	—	18	17	17	17	15	23	23	24	24
Zr	482	465	379	295	163	365	311	163	161	527	736	649	676	675
Nb	34	31	25	25	18	28	29	18	21	33	33	32	38	40
Cs	—	—	18·9	—	—	7·1	17·9	13·2	10·0	9·2	103·1	47·7	8·1	3·2
Hf	—	—	9·6	—	—	8·7	7·0	1·3	1·5	12·9	20·1	19·9	19·0	18·9
Pb	28	18	18	35	42	18	31	30	35	26	20	19	31	31
Th	41	36	32·6	23	20	33	33·5	17·3	15	44·4	45	43	53·1	52·9
U	4	4	11·3	2	3	10	10·4	5·3	5·2	14·7	14·5	12·3	11·3	11·1
La	45	48	54·26	52	31	64·62	55·12	40·96	41·22	62·1	66·63	68·01	80·6	82·34
Ce	121	167	121·51	103	79	139·32	118·56	83·98	83·66	148·4	167·22	168·7	201·22	204·7
Pr			14·72			16·30	13·86	9·13	9·05	18·74	23·31	23·71	26·07	26·59

JOURNAL OF PETROLOGY VOLUME 45 NUMBER 4 APRIL 2004

	Composite dyke 3					Composite dyke 4					Zabrdica		Rudnik	
Sample:	LM VM XII/1	LM VM XII/2	LM VM XII/3	LM VM XII/4	D VM XII/5	LM VM XIV/2	LM VM XIV/4	D VM XIV/1	D VM XI/2	LM VM XIV/6	L ZB01/1	L ZB01/2	L Ro0/1-II	L Ro0/1-A
Nd	62	76	62·22	50	37	67·57	57·09	34·77	33	81·29	97·59	98·92	114·89	116·16
Sm	—	—	10·80	—	—	11·42	9·79	6·06	6·02	13·98	15·73	16·54	19·49	20·69
Eu	—	—	2·15	—	—	2·30	2·01	1·49	1·58	2·45	2·98	2·85	3·28	3·39
Tb	—	—	0·92	—	—	0·99	0·86	0·65	0·68	0·99	1·19	1·23	1·47	1·51
Gd	—	—	7·06	—	—	7·69	6·48	4·74	4·88	8·11	9·58	9·74	11·93	12·11
Dy	—	—	3·63	—	—	3·67	3·33	3·09	3·00	3·36	4·67	4·70	5·28	5·42
Ho	—	—	0·61	—	—	0·62	0·57	0·57	0·55	0·52	0·77	0·77	0·86	0·85
Er	—	—	1·54	—	—	1·63	1·45	1·48	1·45	1·24	1·99	1·95	2·01	2·12
Tm	—	—	0·21	—	—	0·22	0·20	0·22	0·21	0·17	0·30	0·31	0·27	0·27
Yb	—	—	1·38	—	—	1·45	1·27	1·34	1·30	1·10	1·85	1·84	1·75	1·81
Lu	—	—	0·20	—	—	0·21	0·18	0·21	0·20	0·16	0·29	0·27	0·26	0·24

LOI, loss on ignition. L, lamproite; LM, leucominette; D, dacite.

Table 6: Whole-rock Rb, Sr, Nd, Sm, Pb, Th and U concentration (ppm) and Sr, Nd and Pb isotope data recalculated for the given ages

Sample:	ZB01/2	RO/1-II	VM01/3	VM VI/2	VM VI/7	VM XII/3	VM XIV/2	VM XIV/4	VM XIV/6	VM VI/5	VM XIV/1	VM XI/2
Locality:	Zabrdica	Rudnik	V. Majdan	V. Majdan	V. Majdan	V. Majdan	V. Majdan	V. Majdan	V. Majdan	V. Majdan	V. Majdan	V. Majdan
Rock:	lamproite	lamproite	minette	leucominette	leucominette	leucominette	leucominette	leucominette	leucominette	dacite	dacite	dacite
K–Ar age (Ma):*	25·5	30·2	33·5	33·5	33·5	33·5	33·5	33·5	33·5	33·5	33·5	33·5
Rb	194	221	260	380	275	283	226	251	359	191	122	100
Sr	586	598	307	587	418	399	450	491	417	569	346	325
$^{87}Sr/^{86}Sr$	0·711917 ± 6	0·711973 ± 4	0·714162 ± 13	0·710807 ± 5	0·710963 ± 6	0·711137 ± 5	0·710764 ± 5	0·711280 ± 4	0·712072 ± 5	0·709416 ± 5	0·708876 ± 8	0·708870 ± 3
$^{87}Sr/^{86}Sr_{(i)}$	0·71157	0·71152	0·71299	0·70992	0·71006	0·71016	0·71007	0·71058	0·71089	0·70895	0·70839	0·70839
Nd	98·9	114·9	84·3	85·8	77·1	62·2	67·6	57·1	81·3	36·5	34·8	33·5
Sm	16·5	19·5	14·6	15·2	13·9	10·8	11·4	9·8	14	6·6	6·1	6
$^{143}Nd/^{144}Nd$	0·512178 ± 4	0·512208 ± 6	0·512200 ± 4	0·512211 ± 6	0·512235 ± 5	0·512252 ± 5	0·512256 ± 6	0·512261 ± 6	0·512213 ± 5	0·512340 ± 6	0·512357 ± 6	0·512349 ± 5
$^{143}Nd/^{144}Nd_{(i)}$	0·51215	0·51217	0·51216	0·51217	0·5122	0·51221	0·51222	0·51222	0·51218	0·5123	0·51232	0·51231
Pb	19	31	56	74	50	18	18	31	26	32	30	35
Th	43	53·1	18·5	43·7	37·8	32·6	36	33·5	44·4	19·6	17·3	15
U	12·3	11·3	6·2	13·7	13·3	11·3	4	10·4	14·7	7	5·3	5·2
$^{206}Pb/^{204}Pb$	18·701	18·669	18·681	18·639	18·635	18·734	18·678	18·637	18·716	18·625	18·674	18·658
$^{207}Pb/^{204}Pb$	15·667	15·666	15·663	15·685	15·676	15·667	15·653	15·656	15·665	15·663	15·696	15·662
$^{208}Pb/^{204}Pb$	38·812	38·777	38·832	38·844	38·818	38·873	38·797	38·744	38·868	38·776	38·901	38·798

*Cvetković *et al.* (in preparation); subscript i indicates initial values.

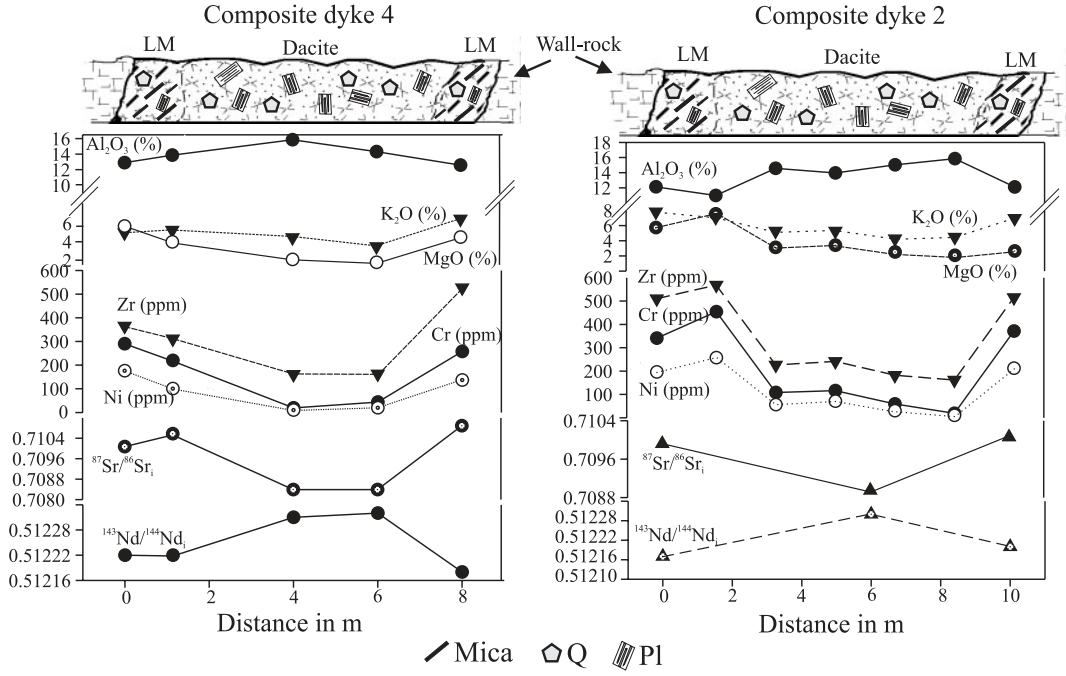

Fig. 7. Characteristic lithological and geochemical cross-sections through composite dykes 2 and 4 from Veliki Majdan. LM, leucominette. Data from Table 5.

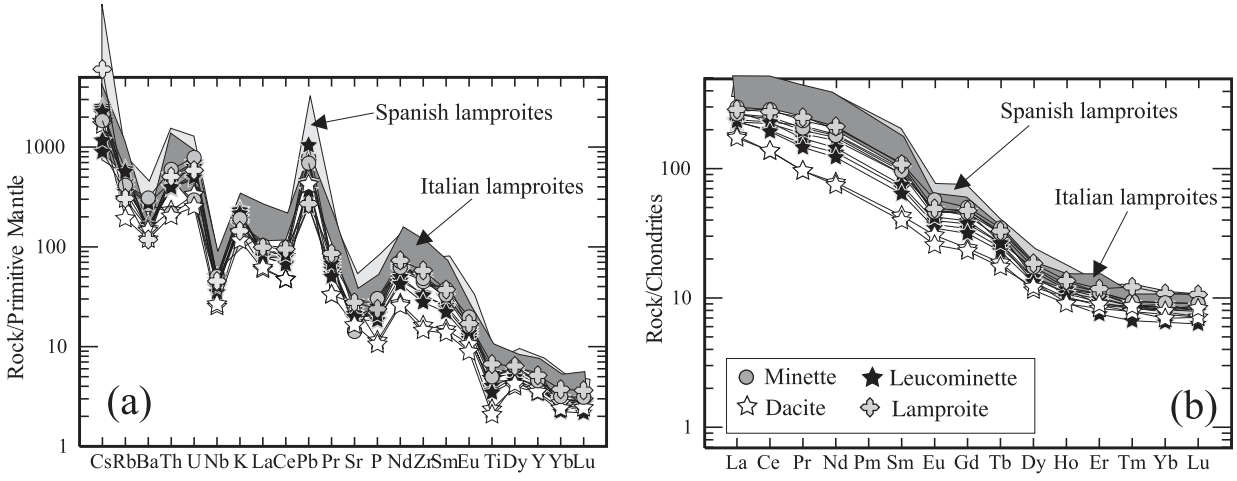

Fig. 8. (a) Primitive mantle-normalized trace element variation diagrams and (b) chondrite-normalized REE patterns for the studied rocks. Coefficients for normalization after Sun & McDonough (1989). Fields for Italian and Spanish lamproites from Conticelli *et al.* (2002) and Turner *et al.* (1999), respectively.

The Pb isotope systematics (Table 6) do not show the significant heterogeneity seen for the Sr–Nd isotopes. Also, no considerable differences and clear isotopic correlation are observed between lamproites, minette, leucominette and dacite samples (Fig. 10c and d). All lithologies are enriched in radiogenic components, with $^{206}Pb/^{204}Pb$ ranging from 18·698 to 18·906, $^{207}Pb/^{204}Pb$ between 15·660 and 15·700 and $^{208}Pb/^{204}Pb$ between 38·843 and 39·070. All analysed samples overlap the pelagic sediments array (Ben Othman *et al.*, 1989), and overlap the Pb isotopic composition of Spanish and Italian lamproites (Turner *et al.*, 1999; Conticelli *et al.*, 2002).

DISCUSSION

Hybridization processes in Veliki Majdan rocks

Petrographic and mineral chemical evidence for hybridization

The mutual coexistence of two magmas is the first precondition for any hybridization processes. On the level of

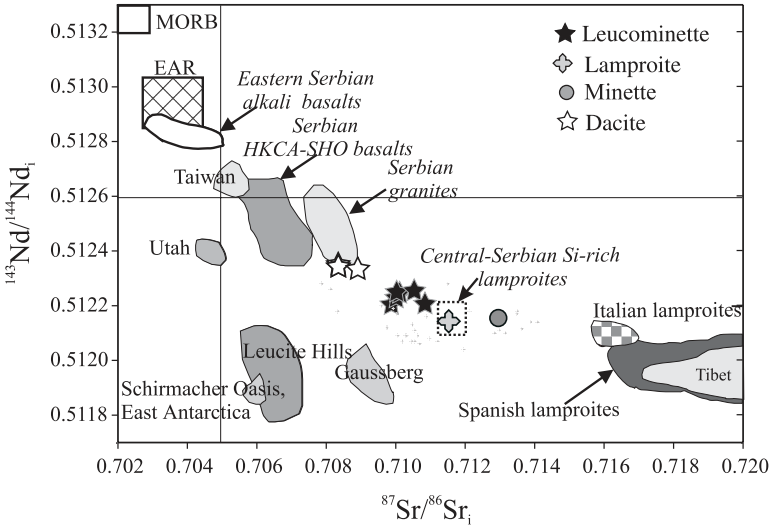

Fig. 9. Sr–Nd isotope diagram for the studied rocks. Also shown for comparison are fields for: Central Serbian Si-rich lamproites (Prelević *et al.*, in preparation); Eastern Serbian alkali basalts (Cvetković *et al.*, in preparation); Taiwan ultrapotassic rocks (Chung *et al.*, 2001); Serbian high-K calcalkaline to shoshonitic (HKCA-SHO) basalts (Cvetković *et al.*, in preparation); Serbian granites (Karamata *et al.*, 1990); Utah lamproites (Tingey *et al.*, 1991; Wannamaker *et al.*, 2000); Schirmacher Oasis, East Antarctica, minette (Hoch *et al.*, 2001); Gaussberg lamproite (Murphy *et al.*, 2002); Leucite Hills lamproites (Nelson *et al.*, 1986); Italian lamproites (Conticelli *et al.*, 2002); Tibet ultrapotassic rocks (Turner *et al.*, 1996; Miller *et al.*, 1999); Spanish lamproites (Benito *et al.*, 1999; Turner *et al.* 1999); mid-ocean ridge basalt (MORB; Zindler & Hart, 1986); European asthenospheric reservoir (EAR; Cebria & Wilson, 1995).

the whole Serbian ultrapotassic province, this is indicated by the presence of composite dykes and lamprophyric xenoliths in dacites and rhyodacites, which show characteristically finely contorted contacts with the host, implying the role of magma mingling. At Veliki Majdan, on a smaller scale, the textures and compositions of minerals, presented above, provide evidence for mixing of magmas rather than mingling. In particular, the micas in the Veliki Majdan rocks indicate hybridization, whereas similar processes have previously been described mostly on the basis of plagioclase or clinopyroxene compositions (e.g. MacDonald *et al.*, 1992; Stimac & Pearce, 1992).

Evidence supporting the mixing history of the Veliki Majdan rocks includes diverging core–rim and phenocrysts–groundmass evolutionary trends recorded by the phlogopite composition from leucominettes, minettes and lamproites. We interpret the similarity of phlogopite phenocryst core compositions in leucominettes, minettes and lamproites (Fig. 4) as a result of their derivation from similar lamproitic parental magma, whereas their diverging trends reflect their differing low-pressure crystallization histories; namely, the morphology and composition of Type 2 phlogopites from minettes and leucominettes may reflect their crystallization from a hybrid magma ['hybrogenic', according to Hibbard (1995)]. This behaviour reflects the whole-rock enrichment of Al_2O_3 as a consequence of contamination of lamproite melt.

The diversity of resorption textures identified in biotite xenocrysts in minettes and the most mafic leucominettes indicates a role for two major processes, incipient melting and phlogopitization, which have in most cases occurred together. The incipient melting of biotite is recognized by resorption and corrosion, by sieve textures and spongy inner portions filled by glass similar to alkali feldspar in composition, and by the exsolution of tiny Ti-magnetite grains (Fig. 5e and f). These textural characteristics record an abrupt and dramatic rise in temperature as a result of incorporation of the biotite in the lamproitic melt, which initiated the incipient melting and triggered its phlogopitization. In some cases phlogopitization proceeded beyond the stage depicted in Figs 5e and 6, resulting in homogeneous high-Al grains (Fig. 5g). Spongy areas in homogeneous high-Al phlogopites (Fig. 5g) occur in minettes, whereas phlogopitization is less intense at a similar degree of incipient melting in more mafic leucominettes (Fig. 5e).

The partial dissolution and incipient melting features indicate that biotite crystals from a dacitic crystal mush were entrained in a higher-temperature mafic melt that invaded the magma chamber. Taking into account the estimated temperatures of these biotites based on the thermometer of Wones & Eugster (1965), the temperature of the hybrid magma during the hybridization process must have been considerably above 950°C (Prelević & Milovanović, 1998). Mineral dissolution rates (Tsuchiyama & Takahashi, 1983; Donaldson, 1985; Tsuchiyama, 1985; Hammouda & Pichavant, 1999) indicate a large impact of this interaction on minerals (other than biotite) originating from the dacitic magma and immersed in the new hybrid. During the hybridization process, all minerals whose liquidus temperatures were

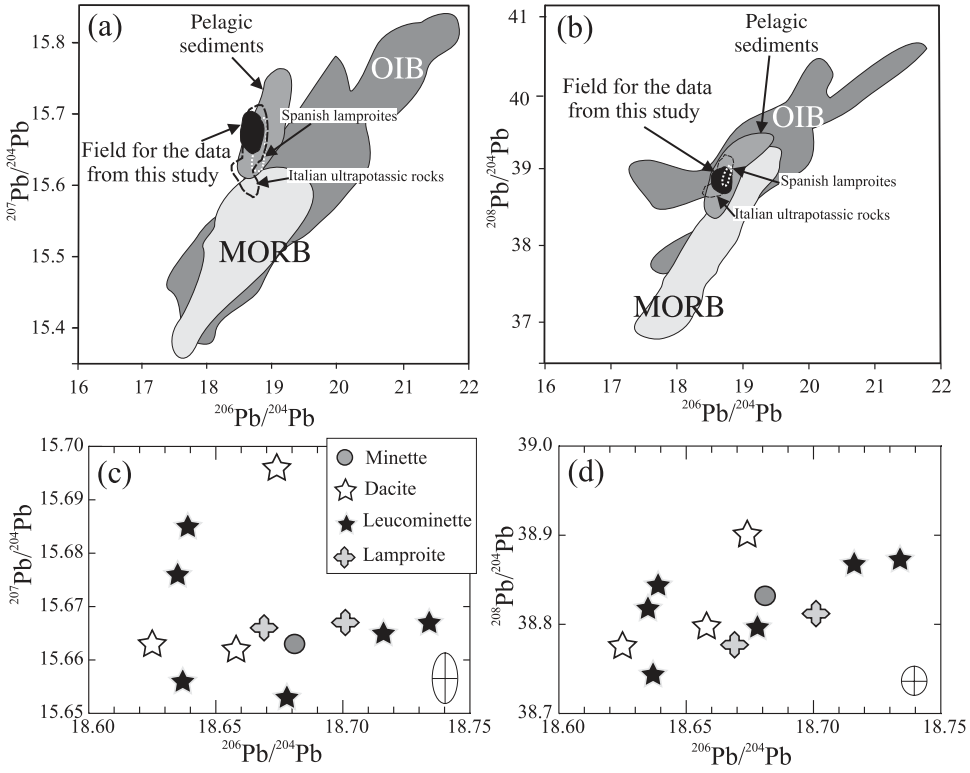

Fig. 10. (a, b) Variation of $^{207}Pb/^{204}Pb$vs $^{206}Pb/^{204}Pb$ and $^{208}Pb/^{204}Pb$ vs $^{206}Pb/^{204}Pb$ for the investigated rocks. Data fields for MORB and OIB from Zindler & Hart (1986) and for pelagic sediments from Ben Othman *et al.* (1989). Data for Mediterranean ultrapotassic provinces same as in Fig. 9. (c, d) Data from this study enlarged.

below that of the hybrid melt would be out of equilibrium and would tend to melt (e.g. quartz, Fig. 2c). This indicates that during the mixing of magmas, the portion of felsic magma entrained in the lamproitic one has been superheated. Moreover, a high volatile content is indicated by the presence of phlogopite throughout the crystallization sequence; this tends to reduce the stability field of feldspars (Yoder & Tilley, 1962), promoting the complete elimination of feldspar phenocrysts in the hybrid magma. The rapid rates of melting of plagioclase relative to quartz in such an environment (Donaldson, 1985; Hammouda & Pichavant, 1999) may explain the very low abundance of plagioclase xenocrysts relative to quartz in the hybrid magma.

The mineralogical, mineral chemical and textural evidence presented above documents an intimate genetic relationship between leucominettes, dacites and minettes by magma mixing and mingling. Furthermore, the textural relationships in Fig. 5f and g suggest that minette is also an integral part of the hybridization sequence and thus is also derived by modification of lamproitic parental melts.

Chemical and isotopic evidence for mixing processes

The choice of the dacite members of the composite intrusions as the silicic end-member for modelling the mixing and hybridization processes is much clearer than the choice of mafic end-member. The origin of the dacites from Veliki Majdan area is related closely to the SiO_2-rich magmatism that gave rise to the nearby Boranja pluton, an I-type granite that forms part of the widespread granitic magmatism of western and central Serbia (Fig. 1) (Cvetković *et al.*, 2000*a*). The depletion of HREE in some dacite samples may be explained by the presence of residual garnet in the source. Melting of metabasites situated in the lower crust would be compatible with this kind of REE pattern.

In Fig. 11, plots of major element oxides and trace elements against SiO_2 or $^{143}Nd/^{144}Nd_i$ indicate that the lamproite samples are located on the apparent continuation of trends defined by the composite intrusions and minettes towards more primitive compositions. Geochemically, therefore, they are the best candidates for the mafic end-member in a magma-mixing model. Conversely, the positive SiO_2 vs Al_2O_3 and negative SiO_2 vs K_2O, and SiO_2 vs Zr/Nb correlations (not shown) are not compatible with the origin of these trends by fractionation of any of the observed mineral phases.

The most convincing evidence for the origin of Veliki Majdan rocks by mixing of dacitic and lamproitic end-members comes from their Sr–Nd isotopic composition, which indicates that melts derived from distinct sources

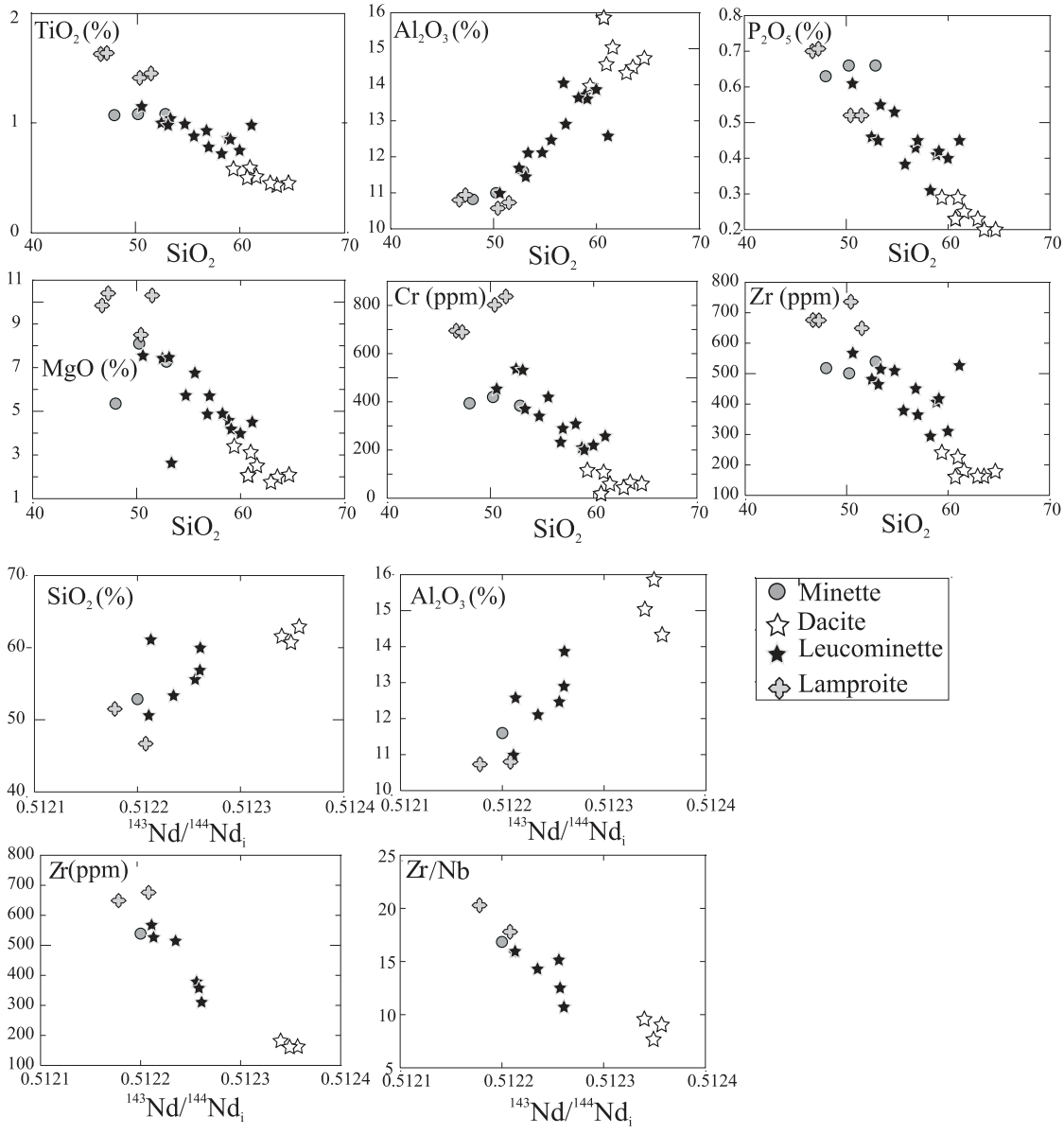

Fig. 11. Variation diagrams for TiO_2, Al_2O_3, P_2O_5, MgO (wt %), Cr and Zr (ppm) vs SiO_2 (wt %) and SiO_2, Al_2O_3 (wt %), Zr (ppm) and Zr /Nb vs $^{143}Nd/^{144}Nd_i$ for the investigated rocks.

were involved in their genesis (Fig. 9). The Sr and Nd isotopic composition of the dacites resembles that of contemporaneous Serbian granites (Karamata *et al.*, 1990; Cvetković *et al.*, 2000*a*), whereas the lamproite samples analysed here are typical for Serbian silica-rich lamproites (Prelević *et al.*, in preparation). Leucominettes clearly occupy the area between the dacitic and lamproitic end-members, lending support to their hybrid origin. The minette sample deviates from the linear trend demonstrated by the other rocks in terms of its higher Sr-isotope ratio, but has a Nd-isotopic ratio consistent with the mixing hypothesis. The deviation to higher $^{87}Sr/^{86}Sr$ for the minette sample can be attributed to alteration of the minette dyke by later deposition of a Pb–Zn ore vein at the contact with Triassic limestone, which is confirmed by the highly radiogenic Sr-isotopic composition of the leachate obtained from the minette sample. The unchanged nature of $^{143}Nd/^{144}Nd_i$ is emphasized by the strong linearity between $^{143}Nd/^{144}Nd_i$ and most elements and element ratios (eg. Zr/Nb) plotted in Fig. 11.

The most reasonable explanation for the lack of any clear correlation between Pb isotopic ratios and some of

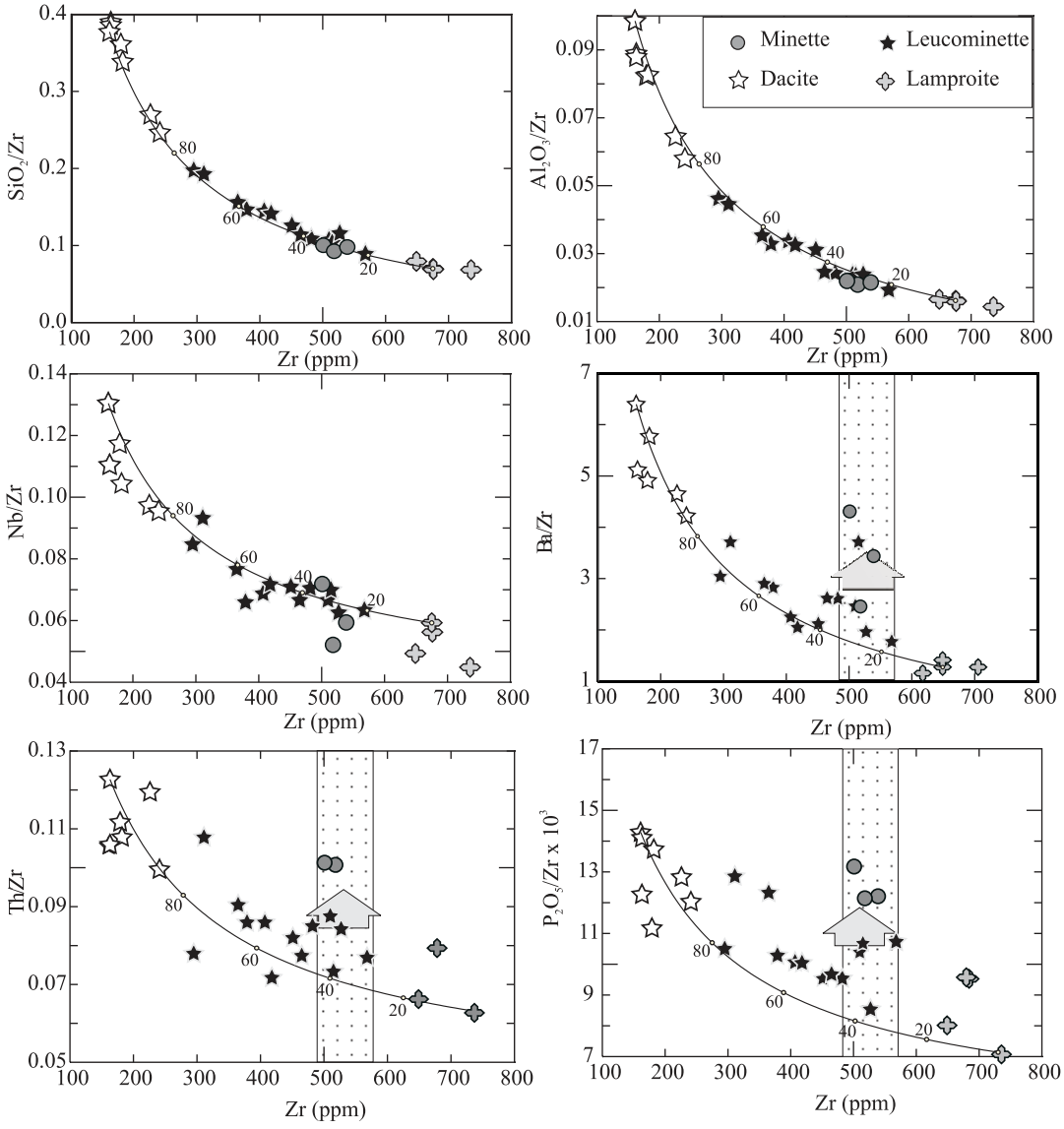

Fig. 12. Selected trace element and major element oxide ratios vs Zr as an index of magma mixing. The dotted area depicts the minette and the most mafic leucominette field, and the grey arrow shows remobilization and enrichment of some elements as a result of volatile retention in the minette magma.

the 'mixing-indices' (SiO_2, Zr, Zr/Nb, $^{143}Nd/^{144}Nd_i$; not shown) recognized in the hybridization model of the Veliki Majdan dykes may be a similarity of the isotopic signature between end-members. Both acid and mafic end-members overlap with respect to their Pb isotope ratios, having a strong crustal signature. Such a signature is to be expected for the acid magmas of clear crustal provenance. On the other hand, Serbian lamproites with the same Pb isotope signature overlap lamproites from Italy and Spain whose geochemical variations and peculiar isotope characteristics have been attributed to crustal contamination of their mantle source (Vollmer, 1976; Rogers *et al.*, 1985; Ellam *et al.*, 1989; Conticelli & Peccerillo, 1992; Peccerillo, 1992).

Modelling of the magma-mixing process shows that selected major and trace element ratios plotted versus Zr plot very close to simple binary mixing hyperbolae (Fig. 12). This confirms that different proportions of the mixing end-members were involved in the formation of the minettes and more mafic leucominettes (20:80 felsic/mafic end-members) to leucominettes (up to 80:20; Fig. 12). The wide range of mixing proportions (20–80%) indicates that magma mixing, and not crustal contamination, must be the process operating, as

assimilation of solid silicic rocks would result in thermal death and solidification of the whole system before such high proportions of crust could be mixed in (Conticelli & Peccerillo, 1992; Peccerillo, 1995; Conticelli, 1998). However, deviations from the mixing trends are shown by minette samples in the case of the Zr vs Ba/Zr, Zr vs P_2O_5/Zr and Zr vs Th/Zr diagrams (Fig. 12), indicative of enrichment in elements with a tendency for volatile-induced redistribution (see below).

Conditions of crystallization and hybridization

Pressure

Rare pargasitic amphibole relicts in leucominette allow calculation of its pressure of crystallization (Table 2). The hornblende barometer based on Al content (Hammarstrom & Zen, 1986) gives the pressure of amphibole crystallization as 6·7–7·0 kbar for the mafic parts of the composite dykes, corresponding to a depth of around 20 km. This pargasitic amphibole is part of the original xenocryst assemblage incorporated into the mafic magma, and is not the product of equilibrium crystallization in lamproite or minette magmas. The stable amphibole in lamproitic melts is K-richterite, and not pargasite, because of low Al_2O_3 contents of the lamproites (Mitchell & Bergman, 1991). Pargasitic amphiboles are also not found in minettes. We infer that these rare relicts of amphiboles originated from the same felsic source as the other xenocrysts in the leucominette host. It follows that the depth indicated by the amphiboles is the maximum depth for the hybridization process.

The role of volatile components

Calcalkaline lamprophyres are rocks with high modal proportions of hydrous mafic minerals, mostly micas and/or amphiboles, indicating an important role for volatiles (Mitchell & Bergman, 1991; Rock, 1991; Mitchell, 1994). The Veliki Majdan minette has a cumulophyric texture and xenomorphic phlogopite grains (Fig. 2e and f); however, there are also quench outgrowths at the corners and edges of some of the large phlogopite plates (Fig. 2f). Rapid crystal growth, forming large crystals, may have been facilitated by high volatile contents, in keeping with the view that some phlogopite macrocrysts in lamprophyres originate by rapid growth in a volatile-rich hybrid melt (Rock, 1991).

The mixing of lamproitic melt with felsic melt did not result in immediate vesiculation, meaning that the hybrid magma was initially water undersaturated. This is indicated by the crystallization of Type 2 Al-rich phlogopite in the leucominette before the formation of the vesicles, which probably occurred during later decompression. This retention of volatiles during and after the mixing process is important in keeping the resultant magmas within the lamprophyre spectrum. The major difference between minette and some of the more mafic leucominettes (leucominette samples that overlap minettes, situated in the stippled area in Fig. 12) is the intensity of phlogopitization of former biotite crystals, which is commonly complete in minette. This may have been facilitated by retained hydrous components, indicating prolonged differentiation of minette in a volatile-rich state, implying growth in an essentially closed system. Furthermore, the retention of water may explain the enrichment of LILE in minettes, whereas increased Th, U, P and light REE (LREE) concentrations may be due to complexing with halogens (Fig. 12).

The compositional resemblance between minettes and more mafic leucominettes (Figs 11 and 12) suggests that they have crystallized from the same hybrid magma type. Leucominettes probably failed to transform into minette because of the ensuing volatile loss during rapid upwelling, which caused degassing of the leucominette mush during withdrawal from the magma chamber.

Theoretical and experimental constraints

There are many theoretical constraints on the processes of magma mixing, especially in the case of interaction between magmas with large compositional contrasts (e.g. Blake & Campbell, 1986; Campbell & Turner, 1986; Wiebe, 1991; Poli *et al.*, 1996). Fluid dynamic experiments have documented two major situations in which mixing may occur (Campbell & Turner, 1986): (1) injection of a pulse of hot dense magma into a less dense, colder, and more viscous magma; (2) establishment of a double diffusive column in a compositionally zoned magma reservoir.

In the first case, the most important factor is the momentum with which a new batch of magma enters the magma chamber; mixing is facilitated by the production of a turbulent fountain, the possibility of which is expressed by a Reynolds number above 400 (Campbell & Turner, 1986). This is potentially the most efficient method of mixing. Detrimental to mixing are a high viscosity contrast, low velocity of the mafic magma invading the magma chamber and high viscosity of the SiO_2-rich magma already residing in the magma chamber, which all serve to considerably depress the Reynolds number. When silicic magma chambers are invaded by 'normal' water-undersaturated basalts, the Reynolds number is too low to induce turbulent mixing (e.g. Campbell & Turner, 1986; Snyder & Tait, 1995).

In the second case, many processes could lead to mingling and mixing of magmas during the approach towards thermal equilibrium (Huppert *et al.*, 1982; Huppert & Sparks, 1988, and references therein). The formation of a compositionally zoned magma chamber is commonly related to the intrusion of a large volume of

basic magma at the base (e.g. Poli *et al.*, 1996), and may result in the formation of hybrid magmas.

The evidence at Veliki Majdan, such as the remarkably variable composition of the mafic parts of the composite dykes, the correlation of reaction textures with the extent of hybridization and the generally small volume of the lamproitic magmatism, favours the first case for mixing involving lamproitic and dacitic magmas.

The high hybridization potential of lamproitic magmas

Lamproite melts may be especially reactive with quartz- and feldspar-bearing rocks or with magmas with high normative quartz contents owing to their high alkali contents and considerable undersaturation in Al_2O_3. Lamproites also have high contents of volatiles that reduce the viscosity and density of the melt. This is indicated by the abundance of phlogopite phenocrysts and suppression of feldspar crystallization in rocks with less than about 55 wt % SiO_2 (Yoder & Tilley, 1962; Burnham, 1979) as well as by analyses of H_2O and F in whole rocks and minerals (Foley *et al.*, 1986*a*, 1986*b*; Edgar *et al.*, 1996). Furthermore, many lamproitic phlogopites have high-pressure characteristics, indicating that high volatile contents are characteristic of lamproite melts near their sources or at lower-crustal levels (Jaques *et al.*, 1986; Foley, 1989; Righter & Carmichael, 1996). Phase equilibrium experiments on minettes and lamproites show that about 3–5% H_2O stabilizes phlogopite, and that even higher contents are required to stabilize it as the sole liquidus phase (Foley, 1990; Righter & Carmichael, 1996).

According to experimental results, alkali-enriched phonolite and trachyte melts with up to 4% H_2O could have viscosities of about 100 Pa s at temperatures of about 1000°C (Whittington *et al.*, 2001). Lamproitic melts should have even lower values, as a result of their high alkali and low Al_2O_3 contents (Bottinga & Weill, 1972; Whittington *et al.*, 2001). Fluorine and water both considerably reduce the effective melt viscosity (Dingwell & Mysen, 1985; Dingwell, 1988), and this may be reduced even further where H_2O is in excess, as is the case for lamproites, so that HF is the dominant fluorine species (Foley *et al.*, 1986*b*). The influence of volatiles on magma density should be even more marked. Because of its high partial molar volume, as well as high coefficients of compressibility and thermal expansion (Lange, 1994; Ochs & Lange, 1997), water may considerably affect magma density, and therefore buoyancy.

A MODEL FOR THE ORIGIN OF THE VELIKI MAJDAN DYKES

The existence of composite intrusions comprising mafic and acid magmas is commonly reported from bimodal magmatic provinces, demonstrating the frequent contemporaneous appearance of melts of contrasting composition (Nemec, 1973; Wiebe, 1984, 1991; Reid & Hamilton, 1987; Perring & Rock, 1991; Fowler & Henney, 1996; Snyder *et al.*, 1997; Wiebe & Ulrich, 1997; Preston, 2001). Two main models have been used to explain the origin of composite intrusions on the basis of geological observations (Wiebe, 1984, 1991; Snyder & Tait, 1995; Snyder *et al.*, 1997; Wiebe & Ulrich, 1997) and from experimental and numerical studies (Carrigan *et al.*, 1992; Carrigan, 1994; Koyaguchi & Takada, 1994). According to the first model, composite dykes are formed when a mafic dyke ruptures a magma chamber filled with silicic magma (Snyder & Tait, 1995; Snyder *et al.*, 1997; Preston, 2001). The second model proposes that composite intrusions are formed by tapping of a compositionally stratified magma chamber (Blake & Campbell, 1986). In both models, the major hybridization episode takes place in a feeder dyke or pipe where the two magmas flow together.

In the case of the Veliki Majdan composite intrusions, several lines of evidence do not favour a single mixing episode, as follows.

(1) Only the dacitic parts of the Veliki Majdan composite dykes (but also discrete dacite dykes) are affected by intense and homogeneous propylitic alteration; the leucominettes and the xenocrysts in them derived from the dacitic magmas are not affected by the alteration. The lack of lateral zonation in hydrothermal mineral paragenesis and in the composition of secondary chlorite shows that there was no thermal gradient, indicating that propylitization was not directly related to the intrusion of the leucominette magma into the composite dyke.

(2) The decimetre-sized transitional zones indicate highly restricted commingling of partly solidified dacite and leucominette magma.

(3) Leucominette itself is a hybrid rock type. The intensity of resorption textures suggesting superheating of silicic magma components incorporated within the lamproitic melt contradicts the one-episode mixing model.

Therefore, we favour a model involving two stages of hybridization for the origin of Veliki Majdan composite intrusions and minette dyke. First, leucominette magma was formed by mixing of lamproitic melt with a silicic magma similar in composition to nearby dacites; subsequently, the intermingling of leucominette and dacite resulted in the chemical gradations in a transition zone between them in the composite intrusions.

Both leucominette and minette are hybrid magmas generated by mixing of lamproitic magma and felsic magma compositionally similar to dacite. The amphibole xenocrysts formed at around 20 km depth indicate that this happened in the lower crust. Our geochemical results imply that virtually every mafic part of the composite dykes resulted from the hybridization of lamproitic and

Table 7: Calculation of parameters influencing the physical conditions of mixing between lamproite melts and the felsic end-member in the Veliki Majdan area

	Lamproitic melt					Felsic end-member	
T (°C)	1200	1200	1200	1200	T (°C)	940	1100
P (kbar)	30	20	10	3	P (kbar)	10	10
wt % H_2O	4	4	4	4	wt % H_2O	4	5
ρ (g/cm^3)	2·91	2·66	2·45	2·32	ρ (g/cm^3)	2·41	2·4
Ø (%)	0	10	20	30	Ø (%)	0	0
$\log_{10}\eta$ (Pa s)	1·07	1·27	1·51	1·82	$\log_{10}\eta$ (Pa s)	4·65	3·9
Q (m/s)		886	632	1428	d (cm)	1000	1000
d (cm)		100	100	150			
Re		1268	480	502	wd/ν	9	70

ρ, density [using model of Lange (1994) and Ochs & Lange (1997)]; Ø, percentage of crystals; η, viscosity (Pa s) [using model of Shaw (1972)]; Q, velocity of the melt (m/s); d, width of feeder dyke (cm); ν, dynamic viscosity ($\nu = \eta/\rho$); $wd/\nu = Q/\nu$, criterion for mixing in the case of high viscosity of silicic melts: when $wd/\nu = 70$, mixing is complete; for values from 70 to 7, mixing is gradually reduced; for values <7, mixing is completely inhibited (Campbell & Turner, 1986). The effects of crystals on the viscosity of melts are calculated using the Einstein–Roscoe relation (Roscoe, 1953). Re, Reynolds number.

dacitic melts in different proportions. Such a situation invokes the presence of many small pulses of silicic magma of different volumes, which migrate from their source either through the dykes (Petford *et al.*, 1993) or by pervasive migration (Weinberg, 1999), rather than the existence of one magma chamber filled with felsic magma. In this scenario, during the invasion of the lamproitic melt, turbulent fountains were able to produce rather homogeneous leucominette hybrids (Eichelberger, 1980; Huppert *et al.*, 1982; Campbell & Turner, 1986; Clynne, 1999). In response to mixing, the hybrid melt reacted with all the phenocrysts originating in the silicic magma, resulting in the reaction textures of the xenocrysts. The most extreme situation is superheating of acid magma batches that are incorporated in the mafic melt, resulting in almost complete elimination of quartz and plagioclase, and causing incipient melting and phlogopitization of biotite xenocrysts.

The hybrid mush cooled and crystallized, resulting in a microporphyritic texture with a low phenocryst/groundmass ratio. Vapour saturation of the resultant leucominette magma caused vesiculation and resulted in extensive, homogeneous propylitization of dacites already residing in the plumbing system. Later batches of hybrid magma also vesiculated producing a mafic foam, considerably lowering its effective density, and inducing buoyancy (Eichelberger, 1980; Huppert *et al.*, 1982). This promoted the rise of leucominette melt into the fractures already occupied by the dacite magma. Vesiculation of the leucominette magma during its ascent is significant in lubricating the viscous silicic magma and producing a pressure gradient that facilitates its upward transport, which would otherwise be strongly inhibited (Carrigan *et al.*, 1992). The minette dyke originated by a similar mixing process, but with volatile retention and phlogopitization of biotite in closed-system late-stage evolution.

Testing the physical conditions of the mixing model

To test the feasibility of the mixing model for the origin of Veliki Majdan intrusions, we estimated key parameters that may control the process of hybridization. The estimated initial conditions are given in Table 7.

The density and viscosity of lamproitic melts with varying crystal contents were estimated assuming 4% of initial H_2O (Righter & Carmichael, 1996) in lamproite sample Zb01/2 from Zabrdica. The initial temperature of the melt is taken to be around 1200°C, based on liquidus experiments on the Gaussberg lamproite, which has similar liquidus olivine and Mg-chromite compositions (Foley, 1985). Estimated densities for the lamproite melt are around 3·0 g/cm^3 and 2·32 g/cm^3 at 30 kbar and 3 kbar, respectively, giving it a strong buoyancy with respect to the upper mantle and the average continental crust (3·30 and 2·75 g/cm^3; Philpotts, 1990). At the point of vesiculation, the effective density of a crystal-bearing foam can drop considerably below 1 g/cm^3 (Huppert *et al.*, 1982).

The viscosity of the lamproite melt was estimated to be as low as 10 Pa s based on Shaw's (1972) model with 4% water and taking most of the Fe to be Fe^{2+}, corresponding to low log f_{O_2} conditions (FMQ − 2·1) estimated from the compositions of coexisting microphenocrysts

of ilmenite and Ti-magnetite from lamproites. Increasing the crystal content from 0 to 30% increases the viscosity to not more than $10^{1·4}$ Pa s at 20 kbar (not shown in Table 7). The velocity of the lamproite melt is estimated to be 223 m/s using the model of Campbell & Turner (1986) for a feeder dyke around 50 cm wide, leading to a Reynolds number of 548 and consequently to turbulent movement within the magmatic feeder.

The high viscosity of the silicic melts may completely inhibit mixing with mafic magma of any type. Phase relationships of melts of dacitic composition suggest a minimum of 4% H_2O for the crystallization of hornblende (Rutherford & Devine, 1988) and temperatures would be not lower than 940°C (Nekvasil, 1991). This allows estimation of viscosity at around $10^{4·6}$ Pa s for the Veliki Majdan dacites (even without phenocrysts) based on Shaw's (1972) model. Using the equation of Campbell & Turner (1986), our estimations show that for such conditions, turbulent mixing with lamproite melt is allowed only if the dacite is devoid of phenocrysts and the temperature of dacite magma rises above 1000°C for a minimum width of the feeder dyke of around 10 m (Table 7), when its viscosity drops below $10^{3·9}$ Pa s. Such a situation is possible if the batches of dacitic magma enclosed by the lamproite melt were superheated by the first batches of lamproitic magma (as suggested on the basis of the biotite reaction textures), facilitating turbulent mixing. Although these values are highly conservative, they confirm that the mixing scenario for the origin of the Veliki Majdan composite intrusions indicated by the mineral chemistry and textures is possible.

Low-viscosity lamproitic melts are able to travel rapidly to shallow depths without losing much heat, and could intrude a silicic magma chamber very rapidly, maintaining its Reynolds number beyond 400, especially in the case of superheating of the silicic melt. Hydrous melts such as lamproites must be potentially the most capable of all mafic melts for creating high Reynolds numbers during intrusion into silicic magma chambers, initiating highly turbulent fountains and causing magma mixing.

APPLICABILITY TO THE ORIGIN OF MINETTES IN GENERAL

Our results demonstrate that hybridization of a lamproite melt with felsic magma led to the production of the Veliki Majdan minette. Prolonged crystallization under volatile-rich conditions resulted in micas with variable compositions that are typical of calcalkaline lamprophyres (Mitchell & Bergman, 1991; Rock, 1991; Mitchell, 1994). The model for the Veliki Majdan minettes may be a globally applicable process for calcalkaline lamprophyres spatially and temporally related to granitic plutonism. The advantage of this locality is the demonstration that lamproites, which are exceptionally reactive with continental crustal rocks, may be an essential component in the formation of minettes. This high hybridization potential of lamproitic magmas means that in other areas they may play a role in lower-crustal hybridization even where they are not seen at the surface. The prerequisites are that the geodynamic setting is suitable for the production of both lamproitic and granitic melts, which are generated in areas of post-orogenic collapse and relaxation that follow convergent tectonics. Post-orogenic granitoids of calcalkaline character are commonly present in such environments (Barbarin, 1999), and lamproites also occur in this setting, particularly in the Mediterranean region, with localities in Serbia (Cvetković *et al.*, 2000*a*; Prelević *et al.*, 2001*b*), southeastern Spain (Venturelli *et al.*, 1984*a*, 1991; Toscani *et al.*, 1995; Benito *et al.*, 1999; Turner *et al.*, 1999), the Italian Alps (Venturelli *et al.*, 1984*b*), and Tuscany (van Bergen *et al.*, 1983; Conticelli *et al.*, 1992), but also in the Andean Cordillera (Carlier *et al.*, 1994, 1997; Carlier & Lorand, 1997). Comparable geodynamic settings apply for lamprophyres associated with granites from western and central Europe in the Variscan orogen (Sabatier, 1991; Gerdes *et al.*, 2000; Ferré & Leake, 2001), as well as Late Caledonian granitic and syenitic plutons (Rock & Hunter, 1987; Fowler & Henney, 1996), where involvement of ultrapotassic melts in magma-mixing processes has been invoked.

In this geodynamic environment, the generation of lamproitic melts is favoured by the recent formation of phlogopite-bearing veins from slab-derived fluids and/or melts in a previously depleted mantle peridotite (Foley & Venturelli, 1989; Foley, 1992). The presence of numerous magma chambers of different volume and composition is favoured by the repetitive switching between extensional and wrench tectonics, which may serve to block the paths of lamproitic melts, which would otherwise rapidly reach the upper crust.

Lamproite melts have high volatile contents, low densities and viscosities, and high hybridization potentials, making interaction with crustal melts rapid and efficient. However, as lamproitic melts are usually of small volume (Mitchell & Bergman, 1991), the mixing may be hardly traceable once it has thoroughly occurred.

The late crystallization of Type 2 phlogopite and evidence for vesiculation during magma ascent demonstrate that the hybrid magmas were still highly charged with volatiles, in contrast to established arguments that rapid cooling would result in exsolution of volatiles immediately after injection of mafic melts into a silicic magma chamber. The retention of volatiles is very important for the further evolution of the hybrid mush, as it allows accumulation of hydrous minerals, which grow rapidly in this environment (Rock, 1991). Minettes are the least

intensely hybridized rocks with less than 30% of the silicic component, but are associated with the most extreme type of resorption textures, suggesting superheating of a silicic crystal mush. Subsequent complete phlogopitization of partly resorbed biotite, together with accumulation of phlogopite crystals, occurred in separate melt batches in a closed system.

Lamproites range in composition from extremely silica-poor (madupitic lamproites) to silica-rich (e.g. sanidine lamproites) magmas with variable Ca and Mg and volatile contents (Mitchell & Bergman, 1991). The mixing model proposed here is more plausible for the petrogenesis of silica-rich lamproites, which are the common types in Mediterranean-type settings (Foley & Venturelli, 1989).

ACKNOWLEDGEMENTS

The authors wish to thank D. Jacob and all members of Greifswald working-group for helpful discussions and suggestions. D.P. is especially grateful to T. Hammouda for essential discussions in the early phases of the study, as well as to D. Harlov for valuable comments. Andreas Kronz is thanked for his assistance during the microprobe analysis. We thank Hilary Downes, Gabriel Carlier and Sandro Conticelli for constructive reviews that significantly improved the paper. Editorial handling by Marjorie Wilson was very helpful. Financial support by the Deutsche Forschungsgemeinschaft (DFG) within the project Fo 181-15 is gratefully acknowledged. We also acknowledge the support of the European Community Access to Research Infrastructure action of the Improving Human Potential Programme, contract HPRI-CT-1999-00008 awarded to Professor B. J. Wood (EU Geochemical Facility, University of Bristol).

REFERENCES

Andersen, D. J., Lindsley, D. H. & Davidson, P. M. (1993). QUILF; a Pascal program to assess equilibria among Fe–Mg–Mn–Ti oxides, pyroxenes, olivine, and quartz. *Computers and Geosciences* **19**, 1333–1350.

Barbarin, B. (1999). A review of the relationships between granitoid types, their origins and their geodynamic environments. *Lithos* **46**, 605–626.

Barnes, S. J. & Roeder, P. L. (2001). The range of spinel compositions in terrestrial mafic and ultramafic rocks. *Journal of Petrology* **42**, 2279–2302.

Benito, R., López-Ruiz, J., Cebriá, J. M., Hertogen, J., Doblas, M., Oyarzun, R. & Demaiffe, D. (1999). Sr and O isotope constraints on source and crustal contamination in the high-K calc-alkaline and shoshonitic Neogene volcanic rocks of SE Spain. *Lithos* **46**, 773–802.

Ben Othman, D., White, W. M. & Patchett, J. (1989). The geochemistry of marine sediments, island arc magma genesis, and crust–mantle recycling. *Earth and Planetary Science Letters* **94**, 1–21.

Blake, S. & Campbell, I. H. (1986). The dynamics of magma-mixing during flow in volcanic conduits. *Contributions to Mineralogy and Petrology* **94**, 72–81.

Bottinga, Y. & Weill, D. F. (1972). The viscosity of magmatic silicate liquids; a model calculation. *American Journal of Science* **272**, 438–475.

Braxton, D. P. & Petersen, E. U. (1999). Thermal aureoles of fossil epithermal systems; a case study from the Calera Vein, Orcopampa, Peru. In: Macharé, J., Benavides, V. & Rosas, S. (eds) *Volumen Jubilar N° 5, 75° Aniversario de la Sociedad Geologica del Peru—Julio 1999*. Lima: Sociedad Geologica del Peru, pp. 81–102.

Brearley, A. J. (1987*a*). A natural example of the disequilibrium breakdown of biotite at high temperature: TEM observations and comparison with experimental kinetic data. *Mineralogical Magazine* **51**, 93–106.

Brearley, A. J. (1987*b*). An experimental and kinetic study of the breakdown of aluminous biotite at 800°C: reaction microstructures and mineral chemistry. *Bulletin de Minéralogie* **110**, 513–532.

Burnham, C. W. (1979). The importance of volatile constituents. In: Yoder, H. S., Jr (ed.) *The Evolution of the Igneous Rocks; Fiftieth Anniversary Perspectives*. Princeton, NJ: Princeton University Press, pp. 439–482.

Campbell, I. H. & Turner, J. S. (1986). The influence of viscosity on fountains in magma chambers. *Journal of Petrology* **27**, 1–30.

Carlier, G. & Lorand, J. P. (1997). First occurrence of diopside sanidine phlogopite lamproite in the Andean Cordillera; the Huacancha and Morojarja dikes, southern Peru. *Canadian Journal of Earth Sciences* **34**, 1118–1127.

Carlier, G., Lorand, J. P. & Kienast, J. R. (1994). Magmatic osumilite in an ultrapotassic dyke, southern Peru; first occurrence. *European Journal of Mineralogy* **6**, 657–665.

Carlier, G., Lorand, J. P., Audebaud, E. & Kienast, J. R. (1997). Petrology of an unusual orthopyroxene-bearing minette suite from southeastern Peru, Eastern Andean Cordillera: Al-rich lamproites contaminated by peraluminous granites. *Journal of Volcanology and Geothermal Research* **75**, 59–87.

Carrigan, C. R. (1994). Two-component magma transport and the origin of composite intrusions and lava flows. In: Ryan, M. P. (ed.) *Magmatic Systems*. New York: Academic Press, pp. 319–354.

Carrigan, C. R., Schubert, G. & Eichelberger, J. C. (1992). Thermal and dynamical regimes of single- and two-phase magmatic flow in dikes. *Journal of Geophysical Research, B, Solid Earth and Planets* **97**, 17377–17392.

Cebria, J. M. & Wilson, M. (1995). Cenozoic mafic magmatism in Western/Central Europe: a common European Asthenospheric Reservoir? *Terra Abstracts* **8**, 162.

Chung, S.-L., Wang, K.-L., Crawford, A. J., Kamenetsky, V. S., Chen, C.-H., Lan, C.-Y. & Chen, C.-H. (2001). High-Mg potassic rocks from Taiwan: implications for the genesis of orogenic potassic lavas. *Lithos* **59**, 153–170.

Clynne, M. A. (1999). A complex magma mixing origin for rocks erupted in 1915, Lassen Peak, California. *Journal of Petrology* **40**, 105–132.

Conticelli, S. (1998). The effect of crustal contamination on ultrapotassic magmas with lamproitic affinity: mineralogical, geochemical and isotope data from the Torre Alfina lavas and xenoliths, Central Italy. *Chemical Geology* **149**, 51–81.

Conticelli, S. & Peccerillo, A. (1992). Petrology and geochemistry of potassic and ultrapotassic volcanism in central Italy: petrogenesis and inferences on the evolution of the mantle sources. *Lithos* **28**, 221–240.

Conticelli, S., Manetti, P. & Menichetti, S. (1992). Mineralogy, geochemistry and Sr-isotopes in orendites from South Tuscany, Italy; constraints on their genesis and evolution. *European Journal of Mineralogy* **4**, 1359–1375.

Conticelli, S., D'Antonio, M., Pinarelli, L. & Civetta, L. (2002). Source contamination and mantle heterogeneity in the genesis of Italian potassic and ultrapotassic volcanic rocks: Sr–Nd–Pb isotope data from Roman Province and Southern Tuscany. *Mineralogy and Petrology* **74**, 189–222.

Cvetković, V., Knežević, V. & Pécskay, Z. (2000*a*). Tertiary igneous formations of the Dinarides, Vardar zone and adjacent regions: from recognition to petrogenetic implications. In: Karamata, S. & Jankovic, S. (eds) *Geology and Metallogeny of the Dinarides and the Vardar Zone, Banja Luka–Srpsko Sarajevo*, pp. 245–253.

Cvetković, V., Prelević, D. & Pécskay, Z. (2000*b*). Lamprophyric rocks of the Miocene Borac Eruptive Complex (Central Serbia, Yugoslavia). *Acta Geologica Hungarica* **43**, 25–41.

Delaloye, M., Lovrić, A. & Karamata, S. (1989). Age of Tertiary granitic rocks of Dinarides and Vardar zone. In: *Extended Abstracts, XIV Congress CBGA, Sofia*, pp. 1186–1189.

Dingwell, D. B. (1988). The structures and properties of fluorine-rich magmas; a review of experimental studies. In: Taylor, R. P. & Strong, D. F. (eds) *Recent Advances in the Geology of Granite-related Mineral Deposits. Special Volume—Canadian Institute of Mining and Metallurgy*. Montreal, Que.: Canadian Institute of Mining and Metallurgy, pp. 1–12.

Dingwell, D. & Mysen, B. (1985). Effects of water and fluorine on the viscosity of albite melt at high pressure: a preliminary investigation. *Earth and Planetary Science Letters* **74**, 266–274.

Donaldson, C. H. (1985). The rates of dissolution of olivine, plagioclase, and quartz in a basalt melt. *Mineralogical Magazine* **49**, 683–693.

Edgar, A. D., Pizzolato, L. A. & Sheen, J. (1996). Fluorine in igneous rocks and minerals with emphasis on ultrapotassic mafic and ultramafic magmas and their mantle source regions. *Mineralogical Magazine* **60**, 243–257.

Eichelberger, J. C. (1980). Vesiculation of mafic magma during replenishment of silicic magma reservoirs. *Nature* **288**, 446–450.

Ellam, R., Hawkesworth, C., Menzies, M. & Rogers, N. (1989). The volcanism of southern Italy: role of subduction and the relationship between potassic and sodic alkaline volcanism. *Journal of Geophysical Research* **94**, 4589–4601.

Esperanca, S. & Holloway, J. (1987). On the origin of mica-lamprophyres: experimental evidence from a mafic minette. *Contributions to Mineralogy and Petrology* **95**, 207–216.

Ferré, E. C. & Leake, E. B. (2001). Geodynamic significance of early orogenic high-K crustal and mantle melts: example of the Corsica Batholith. *Lithos* **59**, 47–67.

Foley, S. F. (1985). The oxidation state of lamproitic magmas. *Tschermaks Mineralogische und Petrographische Mitteilungen* **34**, 217–238.

Foley, S. F. (1989). Experimental constraints of phlogopite chemistry in lamproites; 1, The effect of water activity and oxygen fugacity. *European Journal of Mineralogy* **1**, 411–426.

Foley, S. F. (1990). Experimental constraints on phlogopite chemistry in lamproites: 2. Effect of pressure–temperature variations. *European Journal of Mineralogy* **2**, 327–341.

Foley, S. F. (1992). Petrological characterization of the source components of potassic magmas: geochemical and experimental constraints. *Lithos* **28**, 187–204.

Foley, S. F. & Venturelli, G. (1989). High K_2O rocks with high MgO, high SiO_2 affinities. In: Crawford, A. J. (ed.) *Boninites and Related Rocks*. London: Unwin Hyman, pp. 72–88.

Foley, S. F., Taylor, W. R. & Green, D. H. (1986*a*). The role of fluorine and oxygen fugacity in the genesis of the ultrapotassic rocks. *Contributions to Mineralogy and Petrology* **94**, 183–192.

Foley, S. F., Taylor, W. R. & Green, D. H. (1986*b*). The structural role of fluorine in magmatic systems with application to the genesis of lamproites. In: *Proceedings of the Eighth Australian Geological Convention; Geological Society of Australia; Earth Resources in Time and Space*. Sydney, N.S.W.: Geological Society of Australia, pp. 212–213.

Foley, S. F., Venturelli, G., Green, D. H. & Toscani, L. (1987). The ultrapotassic rocks: characteristics, classification and constraints for petrogenetic models. *Earth-Science Reviews* **24**, 81–134.

Fowler, M. B. & Henney, P. J. (1996). Mixed Caledonian appinite magmas: implications for lamprophyre fractionation and high Ba–Sr granite genesis. *Contributions to Mineralogy and Petrology* **126**, 199–215.

Fraser, K., Hawkesworth, C., Erlank, A., Mitchell, R. & Scott-Smith, B. (1985). Sr, Nd and Pb isotope and minor element geochemistry of lamproites and kimberlites. *Earth and Planetary Science Letters* **76**, 57–70.

Gerdes, A., Woerner, G. & Finger, F. (2000). Hybrids, magma mixing and enriched mantle melts in post-collisional Variscan granitoids; the Rastenberg Pluton, Austria. In: Franke, W., Haak, V., Oncken, O. & Tanner, D. (eds) *Orogenic Processes; Quantification and Modelling in the Variscan Belt. Geological Society, London, Special Publications* **179**, 415–431.

Hammarstrom, J. M. & Zen, E. (1986). Aluminium in hornblende; an empirical igneous geobarometer. *American Mineralogist* **71**, 1297–1313.

Hammouda, T. & Pichavant, M. (1999). Kinetics of melting of fluorphlogopite–quartz pairs at 1 atmosphere. *European Journal of Mineralogy* **11**, 637–653.

Hibbard, M. J. (1995). *Petrography to Petrogenesis*. Englewood Cliffs, NJ: Prentice Hall, 587 pp.

Hoch, M., Rehkamper, M. & Tobschall, H. J. (2001). Sr, Nd, Pb and O isotopes of minettes from Schirmacher Oasis, East Antarctica: a case of mantle metasomatism involving subducted continental material. *Journal of Petrology* **42**, 1387–1400.

Huppert, H. E. & Sparks, R. S. J. (1988). The generation of granitic magmas by intrusion of basalt into continental crust. *Journal of Petrology* **29**, 599–624.

Huppert, H. E., Sparks, R. S. J. & Turner, J. S. (1982). Effects of volatiles on mixing in calc-alkaline magma systems. *Nature* **297**, 554–557.

Jacobs, D. C. & Parry, W. T. (1979). Geochemistry of biotite in the Santa Rita porphyry copper deposit, New Mexico. *Economic Geology and the Bulletin of the Society of Economic Geologists* **74**, 860–887.

Jaques, A. L., Webb, A. W., Fanning, C. M., Black, L. P., Pidgeon, R. T., Ferguson, J., Smith, C. B. & Gregory, G. P. (1984). The age of the diamond-bearing pipes and associated leucite lamproites of the West Kimberley region, Western Australia. *BMR Journal of Australian Geology and Geophysics* **9**, 1–7.

Jaques, A. L., Boxer, G. L., Lucas, H. & Haggerty, S. E. (1986). Mineralogy and petrology of the Argyle lamproite pipe, Western Australia. In: *Proceedings of the Fourth International Kimberlite*

Conference. Sydney, N.S.W.: Geological Society of Australia, pp. 48–50.

Karamata, S. & Krstić, B. (1996). Terranes of Serbia and neighboring areas. In: Knežević Đordjevic, V. & Krstić, B. (eds) *Terranes of Serbia*. Belgrade: Faculty of Mining and Geology, University of Belgrade, pp. 25–40.

Karamata, S., Steiger, R., Djordjević, P. & Knežević, V. (1990). New data on the origin of granitic rocks from western Serbia. *Bulletin, Académie Serbe des Sciences et des Arts, Classe des Sciences Mathématiques et Naturelles, Sciences Naturelles* **32**, 1–9.

Karamata, S., Krstić, B., Dimitrijević, D. M., Dimitrijević, M. N., Knežević, V., Stojanov, R. & Filipović, I. (1997). Terranes between the Moesian Plate and the Adriatic Sea. In: Papanikolaou, D. (co-ordinator) *IGCP Project No 276; Paleozoic Geodynamic Domains and their Alpidic Evolution in the Tethys*. Athens: Geological Laboratory, Athens University, pp. 429–477.

Karamata, S., Dimitrijević, N. M. & Dimitrijević, D. M. (1999). Oceanic realms in the central part of the Balkan Peninsula during the Mesozoic. *Slovak Geological Magazine* **5**, 173–177.

Koyaguchi, T. & Takada, A. (1994). An experimental study on the formation of composite intrusions from zoned magma chambers. *Journal of Volcanology and Geothermal Research* **59**, 261–267.

Lange, R. A. (1994). The effect of H_2O, CO_2 and F on the density and viscosity of silicate melts. In: Carroll, M. R. & Holloway, J. R. (eds) *Volatiles in Magmas*. *Mineralogical Society of America, Reviews in Mineralogy* **30**, 330–369.

Le Bas, M. J., Le Maitre, R. W., Streckeisen, A. & Zanettin, B. A. (1986). Chemical classification of volcanic rocks based on the total alkali–silica diagram. *Journal of Petrology* **27**, 745–750.

Le Maitre, R. W. (ed.) (2002). *Igneous Rocks: A Classification and Glossary of Terms*. Cambridge: Cambridge University Press, 236 pp.

MacDonald, R., Upton, B. G. J., Collerson, K. D., Hearn, B. C., Jr & James, D. (1992). Potassic mafic lavas of the Bearpaw Mountains, Montana; mineralogy, chemistry, and origin. *Journal of Petrology* **33**, 305–346.

Miller, C., Schuster, R., Klötzli, U., Frank, W. & Purtscheller, F. (1999). Post-collisional potassic and ultrapotassic magmatism in SW Tibet: geochemical and Sr–Nd–Pb–O isotopic constraints for mantle source characteristics and petrogenesis. *Journal of Petrology* **40**, 1399–1424.

Mitchell, R. H. (1994). The lamprophyre facies. *Mineralogy and Petrology* **51**, 137–146.

Mitchell, R. H. & Bergman, S. C. (1991). *Petrology of Lamproites*. New York: Plenum, 447 pp.

Murphy, D. T., Collerson, K. D. & Kamber, B. S. (2002). Lamproites from Gaussberg, Antarctica: possible transition zone melts of Archaean subducted sediments. *Journal of Petrology* **43**, 981–1001.

Nekvasil, H. (1991). Ascent of felsic magmas and formation of rapakivi. *American Mineralogist* **76**, 1279–1290.

Nelson, D. R., McCulloch, M. T. & Sun, S. S. (1986). The origins of ultrapotassic rocks as inferred from Sr, Nd and Pb isotopes. *Geochimica et Cosmochimica Acta* **50**, 231–245.

Nemec, D. (1973). Differentiation series of minettes in the Central Bohemian pluton. *Journal of Geology* **81**, 632–642.

Ochs, F. A. I. & Lange, R. A. (1997). The partial molar volume, thermal expansivity, and compressibility of H_2O in $NaAlSi_3O_8$ liquid: new measurements and an internally consistent model. *Contributions to Mineralogy and Petrology* **129**, 155–165.

Peccerillo, A. (1992). Potassic and ultrapotassic rocks: compositional characteristics, petrogenesis and geologic significance. *Episodes—Journal of International Geoscience* **15**, 243–251.

Peccerillo, A. (1995). Mafic calcalkaline to ultrapotassic magmas in central–southern Italy; constraints on evolutionary processes and implications for source composition and conditions of magma generation. In: Cordani, U. G. & Svisero, D. P. (eds) *Proceedings of the Symposium on the Physics and the Chemistry of the Upper Mantle*. Rio de Janeiro: Academia Brasileira de Ciencias, pp. 171–189.

Perring, C. S. & Rock, N. M. S. (1991). Relationships between calc-alkaline acidic and basic (mantle-derived) magmas in late Archaean composite dykes, Kambalda Goldfield, Western Australia. *Precambrian Research* **52**, 245–273.

Petford, N., Kerr, R. C. & Lister, J. R. (1993). Dyke transport of granitoid magmas. *Geology* **21**, 845–848.

Philpotts, A. R. (1990). *Principles of Igneous and Metamorphic Petrology*. Englewood Cliffs, NJ: Prentice Hall, 498 pp.

Poli, G., Tommasini, S. & Halliday, A. N. (1996). Trace element and isotopic exchange during acid–basic magma interaction processes. *Transactions of the Royal Society of Edinburgh: Earth Sciences* **87**, 225–232.

Prelević, D. & Milovanović, D. (1998). Micas of the semilamprophyre/lamprophyric rocks from V. Majdan, Serbia, Yugoslavia. *Annales Géologiques de la Peninsule Balkanique* **62**, 343–367.

Prelević, D., Cvetković, V. & Foley, S. F. (2001*a*). Composite igneous intrusions from Serbia: two case studies of interaction between lamprophyric and granitoid magmas. *Acta Vulcanologica* **13**, 145–157.

Prelević, D., Cvetković, V., Foley, S. F., Jovanović, M. & Melzer, S. (2001*b*). Tertiary ultrapotassic–potassic rocks from Serbia, Yugoslavia. *Acta Vulcanologica* **13**, 101–115.

Prelević, D., Foley, S. F. & Cvetković, V. (2002). Petrology, geochemistry and geodynamic significance of the Serbian ultra-potassic igneous province. *Berichte der Deutschen Mineralogischen Gesellschaft, Beihefte zum European Journal of Mineralogy* **14**, 133.

Preston, R. J. (2001). Composite minor intrusions as windows into subvolcanic magma reservoir processes: mineralogical and geochemical evidence for complex magmatic plumbing systems in the British Tertiary Igneous Province. *Journal of the Geological Society, London* **158**, 47–58.

Reid, J. B., Jr & Hamilton, M. A. (1987). Origin of Sierra Nevadan granite; evidence from small scale composite dikes. *Contributions to Mineralogy and Petrology* **96**, 441–454.

Righter, K. & Carmichael, I. S. E. (1996). Phase equilibria of phlogopite lamprophyres from western Mexico: biotite–liquid equilibria and P–T estimates for biotite-bearing igneous rocks. *Contributions to Mineralogy and Petrology* **123**, 1–21.

Rock, N. M. S. (1977). The nature and origin of lamprophyres: some definitions, distinctions, and derivations. *Earth-Science Reviews* **13**, 123–169.

Rock, N. M. S. (1983). Nature and origin of calc-alkaline lamprophyres; minettes, vosgesites, kersantites and spessartites. *Transactions of the Royal Society of Edinburgh: Earth Sciences* **74**, 193–227.

Rock, N. M. S. (1986). Kimberlite as a variety of lamprophyre. In: Ross, J. (ed.) *Proceedings of the Fourth International Kimberlite Conference*. Sydney, N.S.W.: Geological Society of Australia, pp. 84–86.

Rock, N. M. S. (1991). *Lamprophyres*. Glasgow: Blackie, 285 pp.

Rock, N. M. S. & Hunter, R. H. (1987). Late Caledonian dyke-swarms of northern Britain; spatial and temporal intimacy between lamprophyric and granitic magmatism around the Ross of Mull Pluton, Inner Hebrides. *Geologische Rundschau* **76**, 805–826.

Rogers, N. W., Hawkesworth, C. J., Parker, R. J. & Marsh, J. S. (1985). The geochemistry of potassic lavas from Vulsini, central Italy, and implications for mantle enrichment processes beneath the Roman region. *Contributions to Mineralogy and Petrology* **90**(2–3), 244–257.

Romer, R. L., Foerster, H. J. & Breitkreuz, C. (2001). Intracontinental extensional magmatism with a subduction fingerprint; the Late Carboniferous Halle volcanic complex (Germany). *Contributions to Mineralogy and Petrology* **141**, 201–221.

Roscoe, R. (1953). Suspensions. In: Hermans, J. J. (ed.) *Flow Properties of Disperse Systems*. Amsterdam: North Holland, pp. 1–38.

Rutherford, M. J. & Devine, J. D. (1988). The May 18, 1980, eruption of Mount St. Helens; 3, Stability and chemistry of amphibole in the magma chamber. *Journal of Geophysical Research, B, Solid Earth and Planets* **93**, 11949–11959.

Sabatier, H. (1991). Vaugnerites—special lamprophyre-derived mafic enclaves in some Hercynian granites from Western and Central Europe. In: Didier, J.-P. & Barbarin, B. (eds) *Enclaves and Granite Petrology*. Amsterdam: Elsevier, pp. 63–81.

Shaw, H. R. (1972). Viscosities of magmatic silicate liquids: an empirical method of prediction. *American Journal of Science* **272**, 870–893.

Snyder, D. & Tait, S. (1995). Replenishment of magma chambers: comparison of fluid-mechanic experiments with field relations. *Contributions to Mineralogy and Petrology* **122**, 230–240.

Snyder, D., Crambes, C., Tait, S. & Wiebe, R. A. (1997). Magma mingling in dikes and sills. *Journal of Geology* **105**, 75–86.

Stimac, J. A. & Pearce, T. H. (1992). Textural evidence of mafic–felsic magma interaction in dacite lavas, Clear Lake, California. *American Mineralogist* **77**, 795–809.

Streckeisen, A. (1978). IUGS Subcommission on the Systematics of Igneous Rocks; classification and nomenclature of volcanic rocks, lamprophyres, carbonatites and melilitic rocks; recommendation and suggestions. *Neues Jahrbuch für Mineralogie, Abhandlungen* **134**, 1–14.

Sun, S. S. & McDonough, W. F. (1989). Chemical and isotopic systematics of oceanic basalts; implications for mantle composition and processes. In: Saunders, A. D. & Norry, M. J. (eds) *Magmatism in the Ocean Basins*. *Geological Society, London, Special Publications* **42**, 313–345.

Tingey, D. G., Christiansen, E. H., Best, M. G., Ruiz, J. & Lux, D. R. (1991). Tertiary minette and melanephelinite dikes, Wasatch Plateau, Utah; records of mantle heterogeneities and changing tectonics, Mid-Tertiary Cordilleran magmatism; plate convergence versus intraplate processes. *Journal of Geophysical Research, B, Solid Earth and Planets* **96**(8), 13529–13544.

Toscani, L., Contini, S. & Ferrarini, M. (1995). Lamproitic rocks from Cabezo Negro de Teneta: brown micas as a record of magma mixing. *Mineralogy and Petrology* **55**, 281–292.

Tsuchiyama, A. (1985). Dissolution kinetics of plagioclase in the melt of the system diopside–albite–anorthite, and the origin of dusty plagioclase in andesites. *Contributions to Mineralogy and Petrology* **89**, 1–16.

Tsuchiyama, A. & Takahashi, E. (1983). Melting kinetics of a plagioclase feldspar. *Contributions to Mineralogy and Petrology* **84**, 345–354.

Turner, S., Arnaud, N., Liu, J., Rogers, N., Hawkesworth, C., Harris, N., Kelley, S., van Calsteren, P. & Deng, W. (1996). Post-collision, shoshonitic volcanism on the Tibetan Plateau: implications for convective thinning of the lithosphere and the source of ocean island basalts. *Journal of Petrology* **37**, 45–71.

Turner, S., Platt, J. P., George, R. M. M., Kelley, S. P., Pearson, D. G. & Nowell, G. M. (1999). Magmatism associated with orogenic collapse of the Betic–Alboran domain, SE Spain. *Journal of Petrology* **40**, 1011–1036.

van Bergen, M., Ghezzo, C. & Ricci, C. (1983). Minette inclusions in the rhyodacitic lavas of Mt. Amiata (central Italy): mineralogical and chemical evidence of mixing between Tuscan and Roman type magmas. *Journal of Volcanology and Geothermal Research* **19**, 1–35.

Venturelli, G., Capedri, S., Battistini, G. D., Crawford, A., Kogarko, L. & Celestini, S. (1984*a*). The ultrapotassic rocks from southeastern Spain. *Lithos* **17**, 37–54.

Venturelli, G., Thorpe, R., Piaz, G. D., Moro, A. D. & Potts, P. (1984*b*). Petrogenesis of calc-alkaline, shoshonitic and associated ultrapotassic Oligocene volcanic rocks from the Northwestern Alps, Italy. *Contributions to Mineralogy and Petrology* **86**, 209–220.

Venturelli, G., Toscani, L., Salvioli, M. E. & Capedri, S. (1991). Mixing between lamproitic and dacitic components in Miocene volcanic rocks of S. E. Spain. *Mineralogical Magazine* **55**, 282–285.

Vollmer, R. (1976). Rb–Sr and U–Th–Pb systematics of alkaline rocks; the alkaline rocks from Italy. *Geochimica et Cosmochimica Acta* **40**, 283–295.

Vollmer, R., Ogden, P., Schilling, J.-G., Kingsley, R. & Waggoner, D. (1984). Nd and Sr isotopes in ultrapotassic volcanic rocks from the Leucite Hills, Wyoming. *Contributions to Mineralogy and Petrology* **87**, 359–368.

Wannamaker, P. E., Hulen, J. B. & Heizler, M. T. (2000). Early Miocene lamproite from the Colorado Plateau tectonic province, southeastern Utah, USA. *Journal of Volcanology and Geothermal Research* **96**, 175–190.

Weinberg, R. F. (1999). Mesoscale pervasive felsic magma migration: alternatives to dyking. *Lithos* **46**, 393–410.

Whittington, A., Richet, P., Linard, Y. & Holtz, F. (2001). The viscosity of hydrous phonolites and trachytes. *Chemical Geology* **174**, 209–223.

Wiebe, R. A. (1984). A stratigraphic record of magma mixing and liquid evolution in the Newark Island layered intrusion, Nain, Labrador. In: Dungan, M. A., Grove, T. L. & Hildreth, W. (eds) *ISEM Proceedings of the Conference on Open Magmatic Systems, Fort Burgwin*, Dallas, TX: Institute for the Study of Earth and Man, pp. 166–168.

Wiebe, R. A. (1991). Commingling of contrasted magmas and generation of mafic enclaves in granitic rocks. In: Didier, J.-P. & Barbarin, B. (eds) *Enclaves and Granite Petrology*. Amsterdam: Elsevier, pp. 393–403.

Wiebe, R. A. & Ulrich, R. (1997). Origin of composite dikes in the Gouldsboro granite, coastal Maine. *Lithos* **40**, 157–178.

Wimmenauer, W. (1973). Lamprophyre, Semilamprophyre und anchibasaltsche Ganggesteine. *Fortschritte der Mineralogie* **51**, 3–67.

Wones, D. R. & Eugster, H. P. (1965). Stability of biotite, experiment, theory and application. *American Mineralogist* **50**, 1228–1272.

Woolley, A. R., Bergman, S. C., Edgar, A. D., Le Bas, M. J., Mitchell, R. H., Rock, N. M. S. & Scott Smith, B. H. (1996). Classification of lamprophyres, lamproites, kimberlites, and kalsilitic, melilitic, and leucitic rocks. *Canadian Mineralogist* **34**, 175–186.

Yoder, H. S. & Tilley, C. E. (1962). Origin of basalt magmas. *Journal of Petrology* **3**, 343–532.

Zindler, A. & Hart, S. (1986). Chemical geodynamics. *Annual Review of Earth and Planetary Sciences* **14**, 493–571.

APPENDIX

Analyses of international standards and their recommended values determined by XRF spectrometry on fused discs at the University of Greifswald

Sample:	AGV-1	AGV-1-recommended*	±	BHVO-1	BHVO-1-recommended*	±	STM-1	STM-1-recommended*
SiO_2 (wt %)	58·91	58·84	0·58	49·67	49·94	0·54	59·38	59·60
TiO_2	1·04	1·05	0·05	2·74	2·71	0·06	0·14	0·14
Al_2O_3	16·92	17·15	0·34	13·63	13·80	0·21	18·34	18·40
TFe_2O_3	6·63	6·77	0·19	12·09	12·23	0·20	5·22	5·22
MnO	0·09	0·09	0·01	0·17	0·17	0·01	0·22	0·22
MgO	1·55	1·53	0·09	7·18	7·23	0·22	0·13	0·10
CaO	4·91	4·94	0·14	11·32	11·40	0·17	1·20	1·09
Na_2O	4·30	4·26	0·12	2·27	2·26	0·07	8·91	8·94
K_2O	2·90	2·92	0·37	0·50	0·52	0·04	4·30	4·28
P_2O_5	0·50	0·50	0·03	0·27	0·27	0·03	0·16	0·16
Total	97·75	98·05	1·92	99·84	100·53	1·55	98·00	98·15
Cr	26	10	3	276	†	†	9	4
Ni	21	16	†	113	†	†	1	3
Co	13	15	1	38	45	2	<4	1
V	111	120	11	312	317	12	<1	9
Cu	11	60	6	94	136		6	5
Pb	32	36	5	<2	3	0	15	18
Zn	91	88	9	102	105	5	237	235
Rb	72	67	1	19	11	2	119	118
Ba	1196	1230	16	147	139	14	575	560
Sr	628	660	9	380	403	25	674	700
Ga	20	20	3	20	21	2	36	35
Nb	13	15	†	22	19	†	242	270
Zr	252	227	18	185	179	21	1263	1210
Y	19	20	3	19	28	2	47	46

*http://minerals.cr.usgs.gov/geo_chem_stand/index.html.
†Values are not given.